

# Quenching Massive Galaxies with On-the-fly Feedback in Cosmological Hydrodynamic Simulations

J. M. Gabor,<sup>1\*</sup> R. Davé,<sup>1</sup> B. D. Oppenheimer<sup>2,3</sup> & K. Finlator<sup>4,5</sup>

<sup>1</sup>*University of Arizona, 933 N. Cherry Ave, Tucson, AZ 85721*

<sup>2</sup>*Leiden Observatory, Leiden University, PO Box 9513, 2300 RA Leiden, the Netherlands*

<sup>3</sup>*VENI Fellow*

<sup>4</sup>*University of California, Santa Barbara Physics, Santa Barbara, CA 93106*

<sup>5</sup>*Hubble Fellow*

18 August 2011

## ABSTRACT

Massive galaxies today typically are not forming stars despite being surrounded by hot gaseous halos with short central cooling times. This likely owes to some form of “quenching feedback” such as merger-driven quasar activity or radio jets emerging from central black holes. Here we implement heuristic prescriptions for these phenomena on-the-fly within cosmological hydrodynamic simulations. We constrain them by comparing to observed luminosity functions and color-magnitude diagrams from SDSS. We find that quenching from mergers alone does not produce a realistic red sequence, because 1–2 Gyr after a merger the remnant accretes new fuel and star formation reignites. In contrast, quenching by continuously adding thermal energy to hot gaseous halos quantitatively matches the red galaxy luminosity function and produces a reasonable red sequence. Small discrepancies remain – a shallow red sequence slope suggests that our models underestimate metal production or retention in massive red galaxies, while a deficit of massive blue galaxies may reflect the fact that observed heating is intermittent rather than continuous. Overall, injection of energy into hot halo gas appears to be a necessary and sufficient condition to broadly produce red and dead massive galaxies as observed.

**Key words:** galaxies:evolution – galaxies: luminosity function

## 1 INTRODUCTION

Observations show a distinct bimodality in galaxy colours (Strateva et al. 2001; Baldry et al. 2004; Balogh et al. 2004; Bell et al. 2004; Weiner et al. 2005; Willmer et al. 2006), with massive galaxies today generally being ellipticals having little star formation or cold gas, while less massive galaxies tend to be blue spirals with cold gas. Despite being recognized in the earliest observations of galaxies, the origin of this bimodality remains poorly understood. The lack of galaxies in the region between the red sequence of ellipticals and blue cloud of spirals (often called the green valley) indicates that star formation must be quenched rapidly in order to transform blue galaxies into red ones (Bell et al. 2004; Blanton 2006). The preponderance of active galactic nuclei (AGN) in the green valley suggests that AGN are somehow connected to the process of quenching star formation (e.g. Schawinski et al. 2009). Several physical mechanisms

have been proposed to effect this transformation, with two frontrunners garnering much attention recently: feedback associated with galaxy mergers, and quenching due to virial shock heating of accreted gas. Both of these invoke AGN as a crucial energy source, namely quasars in the former case and radio jets in the latter.

Understanding the origin of massive, passive “red and dead” galaxies remains a problem for models of galaxy evolution. Hydrodynamic simulations of gas-rich galaxy mergers have been shown to induce starbursts and fuel powerful quasars (Hernquist 1989; Barnes & Hernquist 1992; Di Matteo et al. 2005). Observations lend support to the idea of a connection between mergers and powerful AGN (Hutchings et al. 1988; Sanders & Mirabel 1996; Canalizo & Stockton 2001; Bennert et al. 2008; Urrutia et al. 2008; but not all: e.g. Bahcall et al. 1997; McLure et al. 1999; Grogin et al. 2005; Gabor et al. 2009; Georgakakis et al. 2009). In merger simulations, the combination of feedback from star formation and black hole accretion unbinds the gas from the merger remnant, leav-

\* Email: jgabor@as.arizona.edu

ing a red elliptical galaxy devoid of fuel for star formation (Silk & Rees 1998; Springel et al. 2005; Hopkins et al. 2008). This is now colloquially known as “quasar mode” feedback. Observations support various aspects of this picture, including high-velocity outflows from post-starburst galaxies (Tremonti et al. 2007) and QSOs (Feruglio et al. 2010), and a peak in the fraction of AGN host galaxies with colors between the red sequence and blue cloud (e.g. Silverman et al. 2008; Schawinski et al. 2009, but see also Silverman et al. 2009; Xue et al. 2010). Recent work hints that secular processes may induce AGN (Cisternas et al. 2011), but it is not clear whether such AGN alone can quench star-formation in their host galaxies.

The presence of hot X-ray emitting gaseous halos around red and dead galaxies in groups and clusters suggests that these may also be associated with quenching. In this scenario, gas falling into the halo from the intergalactic medium (IGM) collides with stationary hot gas already in the halo. The resulting shock heats the gas to the virial temperature, converting the gravitational energy of infall to thermal energy (cf. Eggen et al. 1962; Silk 1977; Rees & Ostriker 1977; White & Rees 1978). Several recent hydrodynamic simulations show that radiative cooling dominates over this shock heating in dark matter haloes below a rough critical mass of  $\sim 10^{12} M_{\odot}$ , which is suggestively close to the mass at which the color bimodality divides galaxies. Above this critical mass, a stable shock forms and the halo develops a stable hot gas halo (Birnboim & Dekel 2003; Kereš et al. 2005, 2009b). This hot halo will shock heat newly accreting gas, thus stalling the ultimate fuel for star formation (Dekel & Birnboim 2006; Birnboim et al. 2007). Dense filaments of gas may penetrate this hot halo, avoiding the virial heating and providing fuel for star formation, but this is predicted to be uncommon at redshifts less than 2 (Dekel & Birnboim 2006; Ocvirk et al. 2008; Dekel et al. 2009a) because filaments are less dense at late times.

In massive galaxy cluster haloes with peaked density distributions (roughly half of all clusters; Bauer et al. 2005), the hot gas appears to be cooling rapidly via X-ray emission (Fabian et al. 1984), yet UV, optical, and NIR observations indicate only trace levels of star formation (Smith et al. 1997; Crawford et al. 1999; Hicks & Mushotzky 2005; Quillen et al. 2008; Donahue et al. 2010) and little cold gas (e.g. Salomé et al. 2006). Hence some additional heating mechanism must counteract the X-ray cooling; this is the well-known cooling flow problem (Fabian 1994). Observations of X-ray cavities thought to result from powerful radio jets have motivated a picture where a radio AGN in the central cluster galaxy provides this extra heating (McNamara et al. 2000; Fabian et al. 2000; McNamara et al. 2005). As gas cools from the hot halo, some of it accretes onto the massive central black hole, inducing an AGN (Ciotti & Ostriker 1997). The kinetic power emerging via radio jets creates bubbles of typical size  $\sim 10$  kpc (Birzan et al. 2004) in the central regions of the cluster. These bubbles then expand and degenerate into sound waves that effectively isotropize outflow energy and heat the hot intracluster gas on scales  $>30$  kpc (Fabian et al. 2003; Voit & Donahue 2005; Fabian et al. 2006; De Young 2010). From gas cooling to gas heating by the AGN, this entire cycle may repeat itself on  $\sim 10^{8-9}$  yr timescales

(Ciotti & Ostriker 2001). This is now referred to as “radio mode” feedback (Croton et al. 2006).

Mechanisms unrelated to supermassive black holes may provide the additional heating in hot X-ray haloes. Thermal conduction in clusters provides central heating and inhibits cooling instabilities, although it is not sufficient to prevent cooling flows in all clusters (Zakamska & Narayan 2003; Parrish et al. 2009; Ruszkowski et al. 2010). Infalling galaxies or stellar clumps may dynamically heat haloes by transferring gravitational energy to the gas (Dekel & Birnboim 2008; Khochfar & Ostriker 2008; Johansson et al. 2009; Ruszkowski & Oh 2010; Birnboim & Dekel 2010). Whatever the mechanism, the key requirement is to heat up the cores enough to prevent substantial cooling and star formation, while allowing central cooling times less than the Hubble time (or even  $< 1$  Gyr) to persist in a substantial fraction of clusters and groups.

Debate persists about the effectiveness of these proposed quenching mechanisms on scales smaller than a kpc, within a single galaxy. Various simulations use different models for black hole accretion and feedback (Springel et al. 2005; Booth & Schaye 2009; DeBuhr et al. 2009; Levine et al. 2010), and recent work raises doubts that even a powerful quasar could significantly affect star-forming gas throughout a galaxy (DeBuhr et al. 2009, 2010). In radio mode feedback, the observed AGN energy output is generally sufficient to counteract the radiative cooling in clusters or groups (McNamara et al. 2006; Best et al. 2006; Giodini et al. 2010). How this energy is efficiently distributed over space and time to prevent substantial cooling and star formation remains unclear, and cosmological models generally do not include realistic AGN radio jet physics. Hence while supermassive black holes are likely to be responsible for quenching, direct *ab initio* simulations of this process on a cosmological scale remain beyond current reach.

Semi-analytic models (SAMs), which marry analytic prescriptions for baryon physics to merger trees from cosmological simulations of dark matter, have successfully incorporated quenching mechanisms to create reasonable red sequence populations. Among analytic prescriptions for gas cooling and star formation, these models typically incorporate a starburst and bulge growth during galaxy mergers. These merger prescriptions are not enough to make massive galaxies red, so modelers include some suppression of cooling in hot, massive haloes, usually via AGN feedback (Croton et al. 2006; Bower et al. 2006; Somerville et al. 2008). While most SAMs contain such prescriptions, the exact amount of quenching feedback required and the mechanisms by which they operate differ widely among models, possibly because these models must make many assumptions regarding the gas dynamics which can be quite uncertain (Lu et al. 2010; De Lucia et al. 2010).

Hydrodynamic cosmological models follow the gas dynamics directly, but without some explicit quenching mechanisms they generally do not yield a realistic red sequence with appropriate luminosity or mass functions. These models greatly reduce the number of free parameters relative to SAMs by tracking the dynamics of gas inflows and outflows directly, at large computational cost. Although hydrodynamic models directly track the dynamics of galaxy mergers and yield hot gas in massive haloes, they still produce only constantly growing, blue, star-forming galaxies at

the massive end of the mass function. Recent work has begun to include black hole fueling and feedback. These works have focused on reproducing the black hole mass–bulge velocity dispersion ( $M - \sigma$ ) relation, black hole properties, and AGN population properties, with significant successes (e.g. Sijacki et al. 2007; Degraf et al. 2010; Booth & Schaye 2009, 2010). Typical models involve Bondi-Hoyle accretion of surrounding gas by the central black hole, with some assumed fraction of the accreted rest-mass converted to heat in the surrounding gas (Springel et al. 2005; Booth & Schaye 2009). These prescriptions, while pioneering, are poorly constrained and may not properly model the dominant accretion mechanisms (Booth & Schaye 2009; DeBuhr et al. 2009). They also do not focus on producing red sequence galaxies as observed, and have had only limited success doing so.

In this work we also employ hydrodynamic simulations, but we focus on reproducing the observed galaxy population rather than the observed black hole and AGN population. Our approach is therefore somewhat different, in a sense intermediate between fully hydrodynamical simulations and SAMs. Here we simply ask, how is quenching related to the evolutionary properties of galaxies and their halos? We apply heuristic models for quenching by adding energy in various forms to galaxies and their surrounding gas during the evolution of the simulation, and ask which models are successful at producing red and dead galaxies as observed. We do not try to explicitly grow black holes and account for their feedback. In Gabor et al. (2010), we conducted a precursor study on *post-processed* star formation histories, and concluded that both radio mode and quasar mode feedback could in principle produce red galaxies if all future star formation was assumed to be suppressed, but several other attempted mechanisms such as shutting off hot mode accretion or recycled wind mode accretion could not. As such, we now focus particularly on the two popular mechanisms of radio mode and quasar mode, with the goal of determining which one drives the quenching of massive galaxies.

Here, as in Gabor et al. (2010), we compare our simulation results to observations of the galaxy population at redshift  $z \approx 0$ , and leave detailed evolutionary studies for the future. We consider the red sequence in color-magnitude diagrams, and the corresponding red galaxy luminosity function. Due to uncertainties in dust models, we use galaxy stellar mass functions to compare our simulated blue cloud population observations. Our main result is that superwinds induced by galaxy mergers cannot create a red sequence, because galaxies continue to accrete gas from the IGM even after a merger, while our quenching mechanism based on hot halo gas produces a successful match to the observed red galaxy luminosity function. This favors radio mode feedback as the primary driver for the formation of the massive red galaxy population.

We describe the physics of our simulations in §2, including our newly implemented quenching models in §2.1. In §3 we describe the observational data. We compare the results of these new models to observed color-magnitude diagrams (CMDs) and luminosity functions (LFs) for local galaxies in §4. We then consider physical consequences of our models in §5, and discuss future directions in the discussion.

## 2 SIMULATIONS

Our simulations are run with an extended version of the N-body + smoothed particle hydrodynamics (SPH) cosmological simulation code GADGET-2 (Springel 2005), as described in Oppenheimer & Davé (2008). Along with gas cooling and star-formation, our version includes galactic winds tied to the star formation and a chemodynamical model with sources including AGB stars and Type Ia supernovae. In the following subsections, we describe additional modifications to the code to implement quenching of star formation.

For star formation in cold, dense regions, we use the two-phase model of Springel & Hernquist (2003). This model, based on McKee & Ostriker (1977), assumes that any gas particle dense enough to be Jeans unstable contains a hot medium and cold clouds in pressure equilibrium. Stars form from the cold clouds with a characteristic timescale,  $\tau$ . This timescale effectively sets the efficiency of star formation, and Springel & Hernquist (2003) find that  $\tau \approx 2$  Gyrs yields galaxy models that match the observed Kennicutt relation (Kennicutt 1998). The three model components exchange mass, energy, and metals via condensation and feedback from supernovae.

Star-forming gas particles in the simulations spawn star particles with a probability based on the star-formation rate. The resulting collisionless star particle takes on a mass equal to half the original mass of a gas particle. The average gas particle spawns up to two star particles in this stochastic way.

Along with the feedback implicit in the star-formation model, our simulations include an explicit stochastic model of galactic winds (Oppenheimer & Davé 2008). We eject star-forming gas particles from galaxies by giving them a velocity kick  $v_w$  (Springel & Hernquist 2003). The probability that a gas particle will enter a wind in the first place is the mass-loading factor  $\eta$  (the ratio of mass entering winds to the mass of stars formed) times the probability for star formation. In our simulations  $v_w$  is proportional to, and  $\eta$  inversely proportional to, the galaxy circular velocity. These scalings, which arise in the momentum-driven wind model of Murray et al. (2005), are motivated by observations of winds in local galaxies (Martin 2005; Rupke et al. 2005). Once a gas particle enters a wind, we decouple it hydrodynamically until it reaches a density 0.1 times the critical density for star formation (up to a maximum duration of  $20 \text{ kpc}/v_w$ ). This decoupling is intended to represent chimneys through which material can escape easily but that cannot be reliably modeled by the spherically-averaging SPH algorithm.

In order to study the chemical enrichment of galaxies and the IGM, our code includes models for stellar mass loss and Type Ia supernovae, described in Oppenheimer & Davé (2008). As the stellar population represented by a star particle ages, mass loss from AGB stars injects metal-enriched mass to the nearest 3 gas particles based on the mass-loss rates from Bruzual & Charlot (2003). We estimate Type Ia supernova rates for each star particle using Scannapieco & Bildsten (2005), with a prompt and delayed component. Each supernova injects both energy and metal mass into the surrounding gas.

With this treatment of galactic winds, our simulations match broad observations of star-forming galaxies and

the IGM, including the chemical enrichment of the IGM at  $z > 2$  (Oppenheimer & Davé 2006, 2008), the galaxy mass-metallicity relation (Davé et al. 2007; Finlator & Davé 2008), and the luminosity functions of high-redshift galaxies (Davé et al. 2006; Finlator et al. 2007). These simulations do not, however, yield massive red and dead galaxies, and galaxies are far too massive and bright at low redshifts. We require some additional mechanisms to halt star-formation in massive galaxies – the hydrodynamics and feedback models we have described above are insufficient.

## 2.1 Quenching Prescriptions

We incorporate two independent quenching models (which may be combined) into GADGET-2. We are deliberately agnostic about whether supermassive black holes or some other mechanisms provide the energy or momentum in these feedback prescriptions. For the first, we assume that major galaxy mergers ultimately drive the transformation of galaxies from blue to red. We identify mergers in the simulation, and add a kinetic kick to the gas in the merger remnant to expel star-forming gas. This burst of energy mimics the effects of a powerful quasar or starburst (e.g. Di Matteo et al. 2005).

In the second quenching model, we assume that the hot gas haloes surrounding massive galaxies facilitate quenching. We identify these hot, massive haloes in the simulation, then continually add thermal energy to the halo gas in order to cut off the fuel for star-formation. The addition of thermal energy mimics the added heat from radio AGN (e.g. McNamara et al. 2005), unresolved gravitational heating (e.g. Dekel & Birnboim 2008), conduction (e.g. Jubelgas et al. 2004), or cosmic rays (e.g. Guo & Oh 2008).

### 2.1.1 Quenching via galaxy mergers

Our first quenching prescription ties truncation of star formation to galaxy mergers. This requires identifying galaxy mergers within the simulations on the fly, then applying some quenching process to the particles in those mergers. We implement empirically-motivated, high-velocity winds that eject cold gas from merger remnants.

Merger identification is based on our on-the-fly galaxy finder, developed in Oppenheimer & Davé (2008). This algorithm uses a parallel friends-of-friends (FOF) algorithm to group together particles into galaxies. We set the linking length between particles to  $0.06r_s(H(z)/H_0)^{1/3}$ , where  $r_s$  is the mean interparticle separation,  $H_0$  is the Hubble constant ( $70 \text{ km s}^{-1}$ ), and  $H(z)$  is the Hubble parameter as a function of redshift. Oppenheimer & Davé (2008) showed that stellar masses of groups found with this prescription successfully matched those obtained in post-processing with the slower but more physically-motivated Spline Kernel Interpolative Denmax (SKID)<sup>1</sup> algorithm (Kereš et al. 2005). To optimize for speed, we divide the simulation volume into grid cells and only calculate distances between particles in neighboring grid cells. We identify groups independently for each central processing unit, then merge groups split onto adjacent CPUs by checking whether groups separated by less

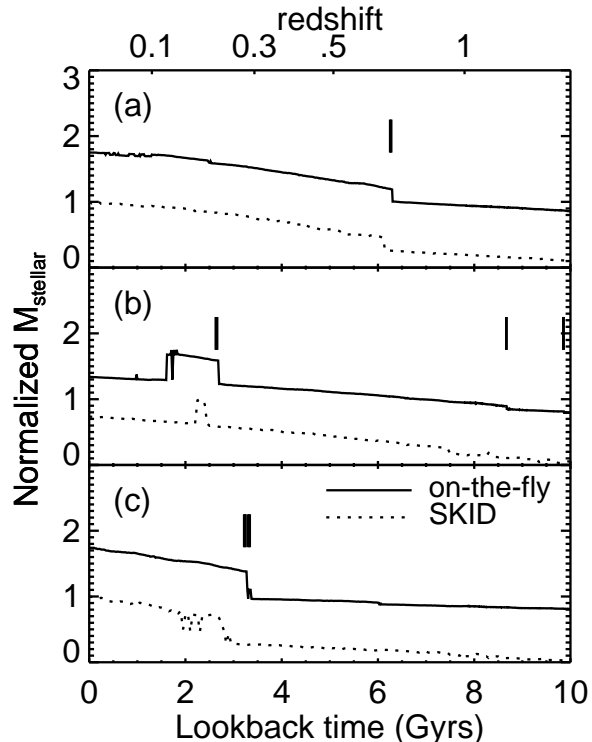


**Figure 1.** Comparison of stellar mass histories calculated using two different group-finders for three galaxies (one galaxy per panel). Dotted lines show normalised masses identified by SKID in post-processing, while solid lines show our faster on-the-fly FOF masses offset by 0.75. Vertical line segments indicate mergers identified on-the-fly. (a) A galaxy with an easily identified major merger. (b) A galaxy with a major fly-by, incorrectly identified as a merger. (c) A merger where the final coalescence is  $\sim 1$  Gyr later with SKID than with our on-the-fly method. The latter two problems are sufficiently rare to have little impact on our results.

than 30 linking lengths indeed have particles that should be linked together. The frequency with which we run the galaxy finder varies from a few Myr to a few 10's of Myr, depending on the adaptive time-step intervals.

We identify mergers on-the-fly by looking for persistent, rapid increases in stellar mass growth. This requires knowing the recent mass history of each galaxy. We track the 6 most recent galaxy catalogs constructed by the galaxy finder, then connect galaxies in the most recent catalog to their earlier most-massive progenitors. By tracking both the current and previous galaxy host of each particle, we can easily identify the progenitors of a given galaxy by searching through its constituent particles and noting their previous host galaxies.

For a given galaxy, we identify a merger by comparing its current stellar mass to that of its recent progenitor galaxy. In detail, we compare the median mass of the three most recent progenitors ( $M_{\text{recent}}$ ) to the median mass of the three older progenitors ( $M_{\text{older}}$ ). If  $M_{\text{recent}}/M_{\text{older}} > (1+1/r)$  then we flag the galaxy as a merger. We use the median approach, rather than just comparing the most recent galaxy mass to the previous one, to avoid declaring mergers of brief encounters and fly-by's. Since the usual value of  $r = 3$  yielded good matches to the galaxy luminosity func-

<sup>1</sup> <http://www-hpcc.astro.washington.edu/tools/skid.html>

tion in Gabor et al. (2010), we use the same choice here (see §4.4 for further discussion).

This method of identifying mergers likely declares the merger before galaxies have fully merged. Since we use all particle types in the galaxy finder, two merging galaxies will appear as one once the central regions of their dark matter haloes overlap. Similarly, when two galaxies closely pass by each other, our method will declare a merger whether the galaxies eventually coalesce or not. Based on the work of Maller et al. (2006), this appears to be a generic problem with merger identification in cosmological simulations. We mitigate this effect partially by taking the median masses over several time steps as described above – rapid fly-by’s will not alter the median mass enough to cause a merger identification, although some longer, close fly-by’s do (as we show below). In cases where the two galaxies do finally coalesce, the precise timing of the quenching does not matter much, since we effectively get rid of all cold gas in the remnant (see below). Early quenching could, however, stunt the star formation that might naturally occur during the merging process, leading to slightly smaller stellar masses and lower metallicities in merger remnants. In the end, our results are not expected to be sensitive to these effects.

To illustrate the successes and challenges of our merger identification method, in Figure 1 we compare the stellar mass histories of galaxies identified on-the-fly to the masses of the same galaxies identified with SKID in post-processing. The mass growth histories from the on-the-fly FOF method broadly match those from SKID, and  $\sim 60\%$  of galaxies with  $M_{\text{stellar}} > 10^{10} M_{\odot}$  in this simulation undergo at least one merger in the last 10 Gyr. Panel (a) shows a well-matched single major merger. Panel (b) illustrates the difficulty with fly-by’s that do not end up merging. Both FOF and SKID combine the two galaxies into a single galaxy at some point, and then separate them again as the two galaxies move apart. Among galaxies with at least one merger, our method mis-identifies fly-by’s as major mergers in  $< 10\%$  of the cases. Panel (c) shows a case where detailed structure in the mass history identified by SKID is missed by FOF. In the FOF case, it looks like a clean-cut major merger. With SKID, however, the stellar mass jumps, then after a few hundred Myrs begins to fluctuate up and down before settling in a more massive state. This suggests an initial fly-by, then a few more close passages, then a final coalescence just over 1 Gyr after the initial merger identification. Among galaxies with at least one merger, our method identifies one of those mergers too early by  $> 500\text{Myr}$  in  $\sim 25\%$ . In future work we may attempt to identify the final coalescence, and avoid mis-identifying fly-by’s, by invoking a delay time of a few hundred Myr before actually declaring the merger. Given the broad nature of this study, such details of merger identification do not substantially affect our results.

Once we have identified a merger, we apply energetic ejective feedback to the star-forming gas within the merger remnant, mimicking a powerful wind. Observations of post-starburst galaxies and QSOs suggest that such winds with velocities  $\sim 1000 \text{ km s}^{-1}$  or more may be responsible for quenching star formation (Tremonti et al. 2007; Feruglio et al. 2010). We pursue the extreme case where all the star-forming gas is ejected in a wind because this is probably necessary to produce a red galaxy remnant (cf. Gabor et al. 2010). Each gas particle in the merger remnant

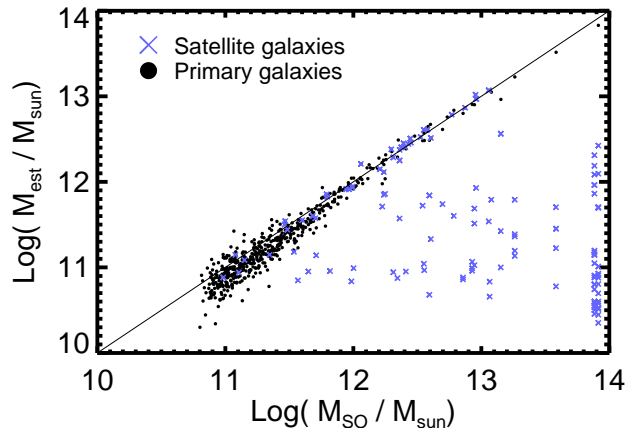


**Figure 2.** Comparison of halo mass estimates from our on-the-fly algorithm ( $y$ -axis) and a post-processing spherical overdensity algorithm ( $x$ -axis). The dotted line shows a perfect 1-to-1 correspondence. In the on-the-fly case, we multiply the baryonic (gas and stellar) mass found by our FOF galaxy finder by an empirical factor of 18 to get  $M_{\text{est}}$  with the best fit. This factor is larger than the expected cosmic factor ( $\sim 6$ ) because we tune the FOF linking length to match the stellar mass, not the total baryonic mass, of galaxies. Much of the baryonic mass remains in an extended halo not captured by the FOF method. The on-the-fly algorithm underestimates the halo masses of many satellite galaxies (blue crosses). This is because the spherical overdensity method associates satellite galaxies with their massive parent halo, whereas our FOF galaxy finder associates them with their smaller sub-haloes.

galaxy is given a velocity kick of  $v_{\text{kick}}$  in the direction  $\vec{v} \times \vec{a}$ , where  $\vec{v}$  is the pre-kick velocity vector, and  $\vec{a}$  is the acceleration vector.

Tremonti et al. (2007) compared post-starburst galaxies with winds  $\sim 1000 \text{ km s}^{-1}$  to low-ionization broad absorption line quasars (Trump et al. 2006) with winds up to  $\sim 10^4 \text{ km s}^{-1}$ . We choose  $v_{\text{kick}} = 1500 \text{ km s}^{-1}$  as a compromise for large-scale outflows that have likely exited the galaxy. Simulations with  $v_{\text{kick}} = 1000 \text{ km s}^{-1}$  showed little difference in the results, since this is still well above the escape velocity for most haloes. As with our winds associated with star-formation, we decouple the wind particles from hydrodynamic processes to enable escape from the ISM, just as we do with star formation-driven winds.

As an addition to ejective feedback, we optionally implemented a thermal feedback mechanism associated with galaxy mergers. In this case, we heat all the star-forming gas particles to the virial temperature of the halo, as estimated below in §2.1.2. It turns out that in combination with the ejective feedback, it makes little difference to the results, since ejected gas almost never returns to the galaxy whether we heat it or not.

### 2.1.2 Quenching in hot haloes

The presence of a hot gaseous halo around most massive red and dead ellipticals hints at some role in quenching. Hence for our second main quenching mechanism, we heat gas in the hot gaseous haloes around galaxies. For each galaxy

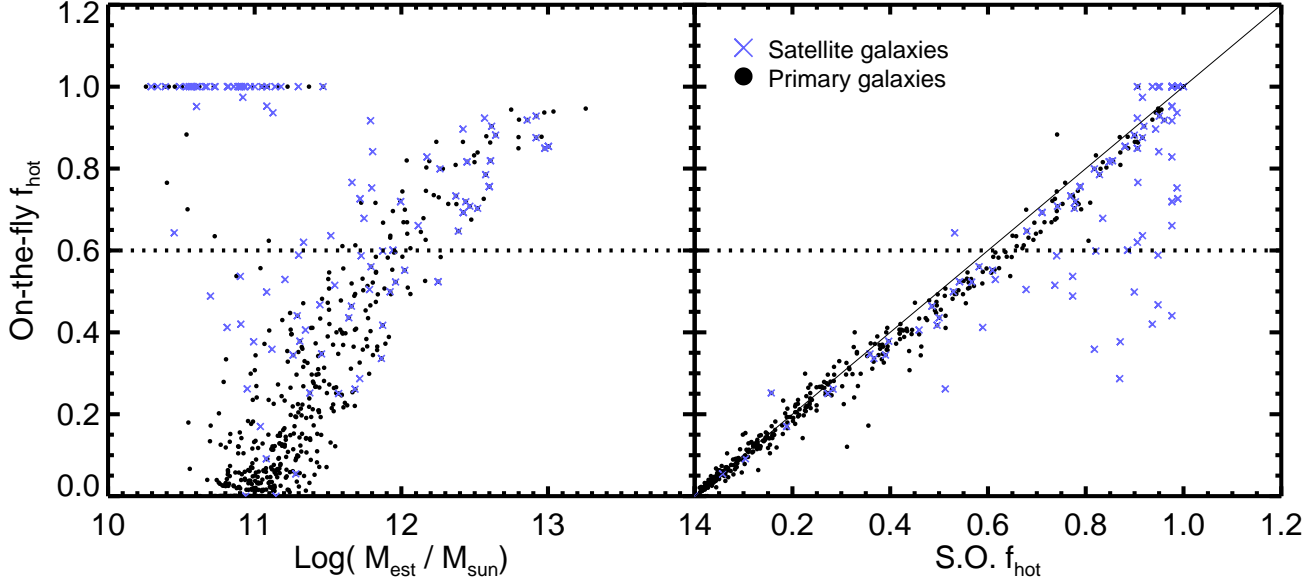


**Figure 3.** Hot gas fractions calculated on-the-fly vs. halo mass ( $M_{\text{est}}$ ) and spherical overdensity (SO) hot fraction for galaxies in a small volume simulation. Black dots show central galaxies and blue crosses satellite galaxies (as found using SO). Hot gas fractions are defined as the fraction of gas within the virial radius above 250,000 K. The left panel shows that low-mass haloes have little hot gas in their surroundings, while increasingly larger haloes have increasingly high hot fractions (cf. Kereš et al. 2005). The galaxies in low-mass haloes with  $f_{\text{hot}} = 1$  are satellite galaxies embedded in massive, hot haloes. The right panel compares our on-the-fly estimate to our post-processing, spherical overdensity estimate of  $f_{\text{hot}}$ , and a thin solid line shows a perfect 1-to-1 correspondence. We can reliably estimate the hot fractions of galaxies on-the-fly in the simulation.

identified on-the-fly, we estimate the hot gas fraction in its halo. In haloes dominated by hot gas, we add heat by raising the temperature of gas particles around the galaxy.

To obtain the hot gas fractions of galactic haloes, we estimate the virial radius corresponding to each halo, find all the gas particles within that radius, then count up the mass on either side of a temperature threshold defining “hot.” We estimate the halo virial radius,  $R_{\text{vir}}$ , using the equation  $\rho_{\text{vir}} = M_{\text{est}} / (4/3\pi R_{\text{vir}}^3)$ . Here,  $\rho_{\text{vir}}$  is the virial density for collapsed structures at the appropriate epoch, and  $M_{\text{est}}$  is an estimated halo mass. We find  $M_{\text{est}}$  by scaling the baryonic mass of the galaxy from the group finder by a factor of 18. As shown in Figure 2, this empirical scale factor value best reproduces the total halo masses found using a more thorough spherical overdensity algorithm in post-processing. This departs significantly from the cosmic value of  $\Omega_M / \Omega_{\text{baryon}} \simeq 6$  because our on-the-fly group finder purposely does not capture the full radial extent of the halo. Our FOF linking length is chosen to match galaxy stellar masses, so it is too small to capture much of the outer halo. Nevertheless, the empirical factor of 18 nicely estimates the total halo mass.

We add the mass of each gas particle within the virial radius to a tally of the hot gas mass if the particle’s temperature exceeds 250,000 K; otherwise, we consider it “cold” or warm for the purpose of identifying hot gas haloes. We choose 250,000 (or  $10^{5.4}$ ) K because this separates the main bulk of cooler IGM that eventually cools into galaxies from the hot tail of the IGM from which cooling and forming stars is rare (cf. Kereš et al. 2005, 2009b; Gabor et al. 2010).

Once we have measured the hot and cold gas masses within the virial radius of each galaxy, we apply the quench-

ing heat if  $f_{\text{hot}} \equiv m_{\text{hot}} / (m_{\text{hot}} + m_{\text{cold}}) > 0.6$ . A hot fraction of 0.6 corresponds roughly to halo masses of  $10^{12} M_{\odot}$  (Kereš et al. 2005). In Gabor et al. (2010), we found that quenching star formation in haloes with  $M > 10^{12} M_{\odot}$  or  $f_{\text{hot}} > 0.6$  led to luminosity functions that best reproduce those observed.

Figure 3 illustrates the effectiveness of our hot fraction estimate in a small simulation. Our on-the-fly hot fraction calculation accurately reproduces the trend noted by Kereš et al. (2005): halos above  $\sim 10^{12} M_{\odot}$  have hot fractions above  $\sim 0.6$  (left panel), and the transition between halos dominated by cold and hot gas is fairly abrupt. Outliers from the trend with low masses and  $f_{\text{hot}} = 1$  are small satellite galaxies embedded in the hot halo of a larger galaxy. In the right panel, we compare our on-the-fly hot fraction estimate to that from our post-processing, spherical overdensity method. With a high degree of reliability, we can determine whether the gaseous halo surrounding a galaxy is hot.

In FOF galaxies above the hot fraction threshold, we raise gas particles to the estimated virial temperature of the halo. In our base model, we only raise the temperatures of particles that are *not* star-forming, i.e. that are not within the existing cold ISM of galaxies within the halo. We also do not raise the temperature of particles already exceeding the virial temperature. We use equation 59 from Voit (2005) to estimate the virial temperature, using  $M_{\text{est}}$  for the halo virial mass:

$$k_B T = (8.2 \text{ keV}) \left( \frac{M_{\text{est}}}{10^{15} h^{-1} M_{\odot}} \frac{H(z)}{H_0} \right)^{2/3}. \quad (1)$$

Here,  $k_B$  is Boltzmann’s constant,  $H(z)$  is the redshift-

dependent Hubble parameter, and  $H_0$  is the Hubble constant (at  $z = 0$ ). In practice, we found that instantaneously heating particles to the virial temperature sometimes led to unphysically high hydrodynamic accelerations. To prevent adaptive time-steps from becoming too short, we instead double the entropy of the gas particle until it reaches the virial temperature. Through this heating mechanism, we prevent gas from ever cooling and forming stars.

A key aspect of our mechanism is that energy is continually added to keep particles hot. Gas within the hot halo that cools below  $T_{\text{vir}}$ , or accreted gas that is below  $T_{\text{vir}}$ , is heated as described above during every time step of the simulation. This is perhaps overkill; to suppress star formation, it may not be necessary to keep gas at or above the virial temperature, nor to do so at every timestep. Here, however, we will make this maximal heating assumption to ensure star formation is suppressed, even though we will discuss later that the energetics of this are quite extreme. We will explore relaxing the heating assumption in future work.

Given the overall success of our hot gas quenching model, we explored many variants on our base model:

(i) We heat *all* gas within halos to the virial temperature, including star-forming gas within the ISM of galaxies.

(ii) We use a criterion based directly on the halo mass (rather than hot gas fraction). While there is a close correlation between hot gas haloes and massive dark matter haloes (cf. Figure 3, Birnboim & Dekel 2003; Kereš et al. 2005), some models have had success quenching star formation above a particular halo mass, typically around  $10^{12} M_{\odot}$  (e.g. Cattaneo et al. 2006; Gabor et al. 2010).

(iii) We restrict the heating to within a certain radius  $r_{\text{heat}}$  from the center of the halo. This is an attempt to mimic feedback from a central radio AGN. Voit & Donahue (2005) argue, based on observations of an entropy floor within the central 30 kpc in cooling flow clusters from Donahue et al. (2006), that an AGN outburst sufficient to counteract the cooling will create subsonic, buoyant bubbles at a typical radius of 30 kpc. The region outside this radius should be heated by the expanding bubbles. Following this, we use  $r_{\text{heat}} = 30$  kpc. A numerical difficulty with this is that we found that large galaxies in our simulations have star-forming regions at significantly larger radii. This result occurs for galaxies identified using both FOF and SKID methods. This may owe either to satellite galaxies at these radii being grouped into the central galaxy, or to the threshold density for star formation being too low. We note that the SF threshold is  $\approx 0.1 \text{ cm}^{-3}$ , which is well below ISM densities where star formation occurs in reality. This is a historical numerical convenience motivated by the inability of our simulations to fully resolve ISM densities. In any case, this variant produces a red sequence, but has too many massive galaxies remain blue due to the ongoing star-formation. Apparently in our simulations, heating only the central regions of a halo does not heat the outer regions as suggested by observations of sound waves in clusters (Fabian et al. 2006). The failure of central heating to spread energy to large radii may suggest that we do not adequately resolve the hydrodynamics in our typical hot haloes, or that raising the temperature to only  $T_{\text{vir}}$  may be insufficient, and we need to raise it further.

(iv) We do not heat gas below our 250000 K critical tem-

perature. This is intended to allow for cold flows from IGM filaments to penetrate into hot haloes, as has been argued by Dekel et al. (2009b). We discuss this variant further in §4.3.

(v) We do not heat gas within sub-haloes. As indicated by Figure 2, many small satellite galaxies live in the hot gas haloes of their larger hosts. AGN in these small galaxies may or may not contribute significantly to the overall heating of the hot gas halo. Since their importance in quenching massive galaxies is debatable, we implemented a method to identify these sub-haloes and exclude them from the feedback prescription. When calculating hot gas fractions as described above, we estimate the virial radius of each FOF galaxy. If a galaxy’s center falls within the virial radius of another, more massive, galaxy, then we consider it a sub-halo. Once we identify sub-haloes, we do not apply the thermal feedback to gas within them. We discuss results of this mechanism in §4.3.

## 2.2 Simulation parameters

Simulating massive galaxies presents a substantially larger computational challenge than simulating more common systems. One is pushed towards larger volumes ( $\gtrsim 50 \text{ Mpc}/h$ ) by the need to obtain a sufficient statistical sample of massive galaxies. Conversely, since massive galaxies begin forming stars first, this requires simulations that robustly resolve early star formation, requiring higher resolution ( $\sim \text{few kpc}$ ). Given computational resource limitations, we can only perform a few large runs. To explore all the variants listed above, we are forced to run smaller simulations. We choose to compromise on volume to ensure robust star formation histories.

Our primary simulations use a box size of  $48h^{-1} \text{ Mpc}$  and a gravitational softening length of  $3.75h^{-1} \text{ kpc}$  (equivalent Plummer), with  $256^3$  dark matter and  $256^3$  gas particles. This yields a gas particle mass of  $1.2 \times 10^8 M_{\odot}$ , and a dark matter particle mass  $5.1 \times$  larger. Our smaller simulations keep the same mass and spatial resolution, but reduce the box size to  $24h^{-1} \text{ Mpc}$  with  $128^3$  dark matter and  $128^3$  gas particles. All simulations and analyses use a *Wilkinson Microwave Anisotropy Probe* concordance cosmology (Komatsu et al. 2009) with  $H_0 \equiv 100h = 70 \text{ km s}^{-1} \text{ Mpc}^{-1}$ , matter density  $\Omega_m = 0.28$ , baryon density  $\Omega_b = 0.046$ , a cosmological constant with  $\Omega_{\Lambda} = 0.72$ , root mean square mass fluctuation at separations of 8 Mpc  $\sigma_8 = 0.82$ , and a spectral index of  $n = 0.96$ . Our small runs are useful for testing some of the variations in the quenching physics, and also for tracking details of each on-the-fly galaxy and feedback event. The larger simulations do a much better job of sampling the massive end of the luminosity function, but take many weeks to run.

We focus primarily on three models which we refer to as *no quenching*, *merger quenching*, and *hot gas quenching*. The no quenching model includes star formation and momentum-conserving winds, but no additional explicit feedback mechanism. It is effectively the same model as the “vzw” model of Oppenheimer & Davé (2008). The merger quenching model incorporates  $1500 \text{ km s}^{-1}$  winds from merger remnants to quench star formation. For the hot gas quenching, we focus on a model where we heat only the non-star-forming gas particles in FOF galaxies with  $f_{\text{hot}} > 0.6$ .



In §4 we will also explore some simulations with slight variations of the quenching models.

### 2.3 Simulation outputs and analysis tools

We output snapshots of each simulation at 108 redshifts, starting at  $z = 30$  and ending at  $z = 0$ . The snapshots contain information for every simulation particle, including position, velocity, mass, metallicity, gas density, gas temperature, star-formation rate, and time of formation (for star particles). In addition to these outputs, we save the galaxy catalog from each instance of the on-the-fly galaxy finder for later analysis.

Our suite of analysis tools allows us to compare our simulation results directly with observations. SKID provides a list of member particles (star and star-forming gas) for each simulated galaxy. The sum of star particle masses is then the galaxy stellar mass, and the star formation rates of the gas particles are summed to give the star formation rate of the galaxy.

We then calculate galaxy spectra using the models of Bruzual & Charlot (2003). We treat each star particle as a single stellar population with an age and metallicity determined directly in the simulation. By adding up the spectra of all star particles within a galaxy, we obtain the spectrum of that galaxy. Then we convolve galaxy spectra with observational filter curves to obtain broad-band colors and magnitudes.

## 3 OBSERVATIONAL CONSTRAINTS

To characterize the effectiveness of our quenching models, we compare the results of our simulated galaxy populations to galaxy observations in the low-redshift ( $z < 0.1$ ) universe. Our goal is to create a realistic red sequence, so we focus on color-magnitude diagrams (CMDs) and red-galaxy luminosity functions (LFs).

We follow Gabor et al. (2010) in using the low-redshift version of the Value-Added Galaxy Catalog (VAGC, Blanton et al. 2005) of the SDSS (Adelman-McCarthy et al. 2008; Padmanabhan et al. 2008). This catalog includes  $ugriz + JHK$  absolute magnitudes for  $\sim 170000$  galaxies with  $z \lesssim 0.05$ . After converting absolute magnitudes to our preferred cosmology (with  $h = 0.70$ ), we can straightforwardly plot CMDs. We will plot  $g-r$  vs  $r$  because the  $r$ -band light is a good tracer of stellar mass. For the luminosity functions, we use  $r$ -band luminosities and the  $1/V_{\max}$  method (Schmidt 1968) with the  $V_{\max}$  values in the VAGC. We compare these observational results with simulation snapshots at  $z = 0.025$ , which we will refer to as low redshift or  $z = 0$ .

As discussed in Gabor et al. (2010) and §4.2, uncertainties in dust obscuration motivate us to compare mass functions (MFs) of blue galaxies rather than luminosity functions. For this we use publicly available stellar masses derived for SDSS galaxies by fitting observed galaxy spectra to templates (Kauffmann et al. 2003b). We cross correlate this sample with the VAGC to obtain  $\sim 40000$  galaxies with stellar masses and broad-band colors for the MFs.

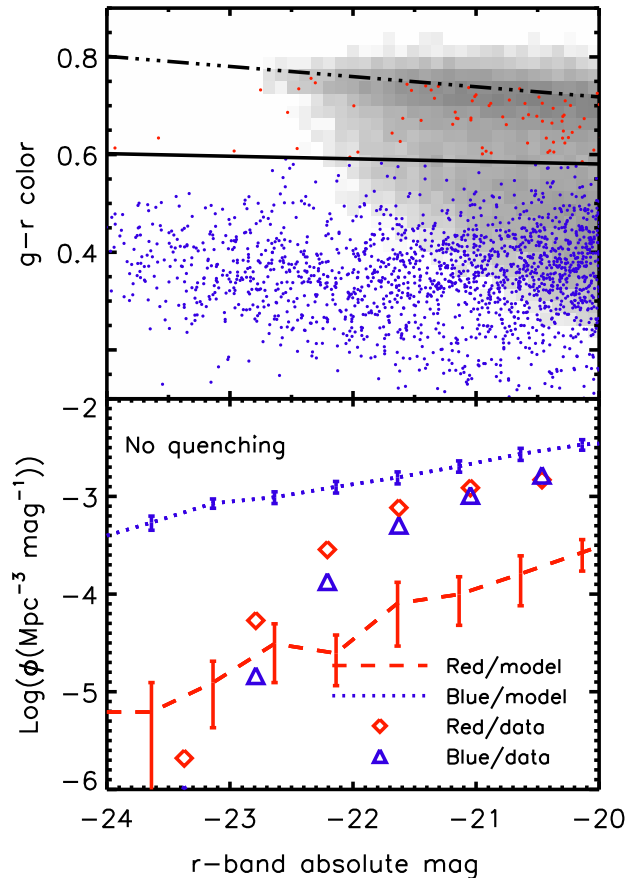


**Figure 4.** CMD (top panel) and LF (bottom) for a simulation with no quenching. In the CMD, grayscale represents the density of SDSS galaxies, points are simulated galaxies, the dot-dashed line is a fit to the observed red sequence, and the solid line separates the simulated red sequence and blue cloud. Without quenching, our simulations do not produce red galaxies. In the LF, symbols represent the observed luminosity functions for red and blue galaxies, and lines are for simulated galaxies. The red galaxy luminosity function is too low by roughly an order of magnitude. Simulated blue galaxy luminosities are computed without a correction for dust to distinguish the intrinsic red sequence more easily.

## 4 CONSTRAINING QUENCHING MODELS

### 4.1 Basic models: Red Galaxies

Since our goal is to reproduce a realistic red sequence, we compare the red galaxy CMDs and LFs produced by our various models to determine the best match. We first illustrate the problem with simulations that do not have additional quenching mechanisms. Figure 4 shows the full CMD and LF for a simulation with no quenching feedback, compared to observations. Following Gabor et al. (2010), we separate red simulated galaxies from blue in the CMD using the solid line. This line is bluer and shallower than that used for observed galaxies because it better captures the bimodality in our most successful models. As we discuss below (and in Gabor et al. 2010), our model red sequence is generally too blue and has little or no slope. We estimate LF uncertainties based on a jackknife re-sampling of the simulation



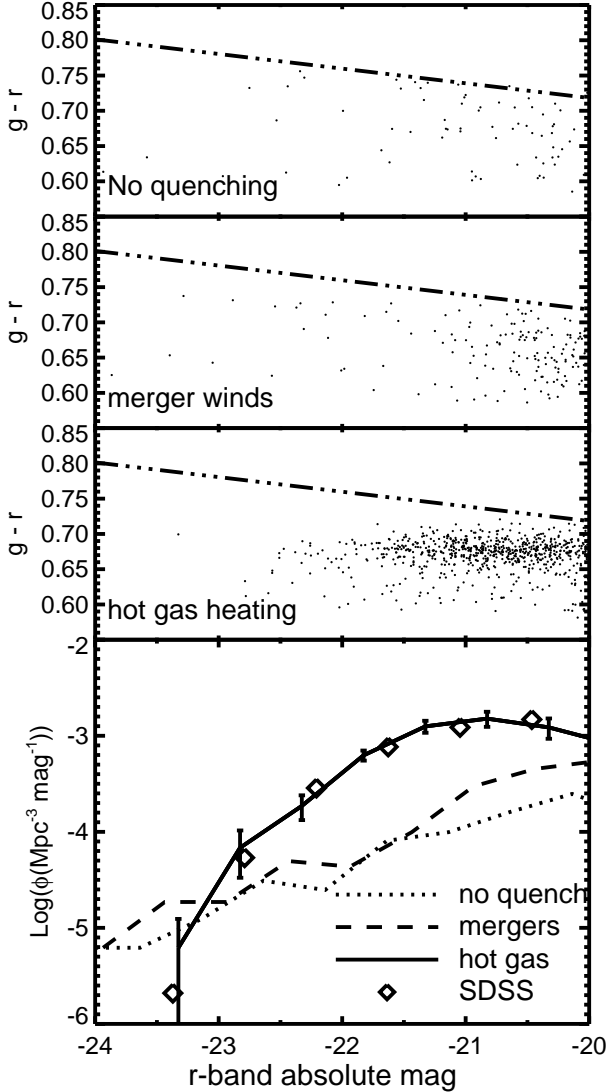


**Figure 5.** CMDs zoomed in on the red sequence (top 3 panels) and LFs (bottom panel) for simulations with no quenching, merger quenching, and hot gas quenching. This shows the main result of this work: merger quenching fails to produce a substantial red sequence, whereas hot gas quenching succeeds.

volume (Finlator et al. 2006) (typical observational uncertainties are smaller than the symbols except for the brightest bins).

Almost all galaxies in this no-quenching simulation constantly accrete gas from the IGM, and this gas supplies the fuel for ongoing star formation. As a result, the simulation produces few red galaxies and many very massive, very bright blue galaxies. The LF reflects this effect. The red galaxy LF is too low (relative to that observed) by an order of magnitude for  $r \approx -21.5$ , and the blue LF is too high. Furthermore, this model does not produce the observed sharp turnover in the luminosity function at high masses (Oppenheimer et al. 2010).

We show the simulated blue galaxies without accounting for obscuration from dust to illustrate the intrinsic galaxy luminosities. Dust obscuration will push the blue galaxies up and to the right (redder and fainter) in the CMD,

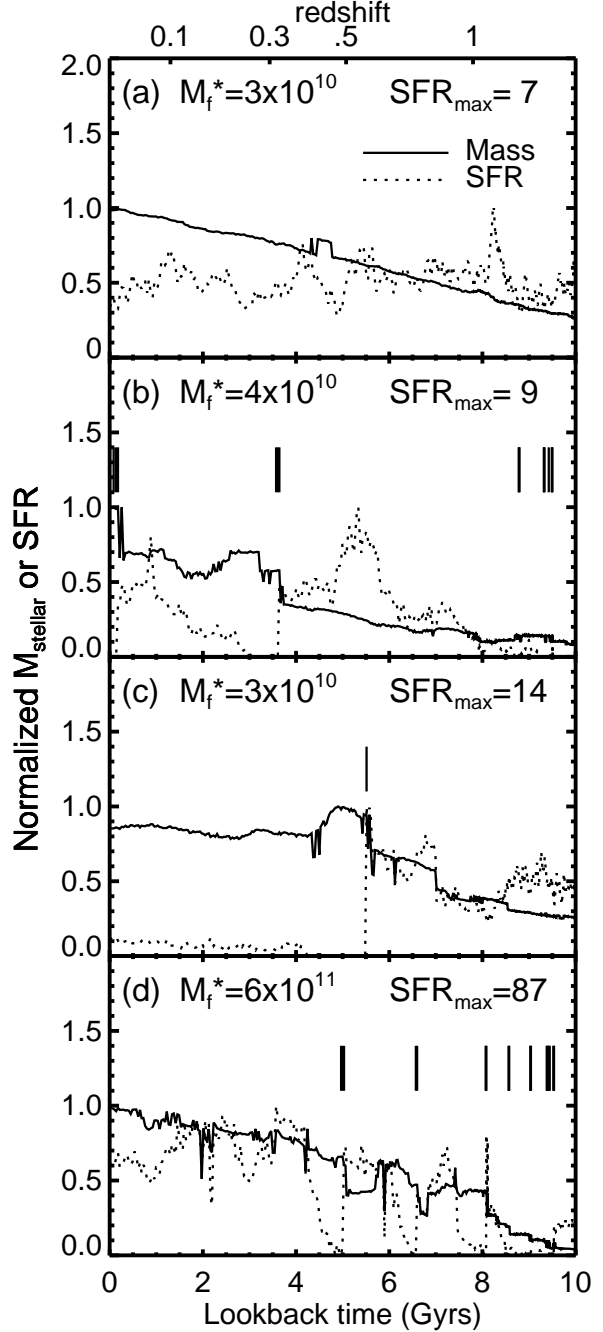


**Figure 6.** Cosmic histories of mass (solid lines) and instantaneous star-formation rate (dotted lines) for 4 galaxies selected from a simulation with merger quenching. These illustrate the variety of outcomes following major mergers. Vertical solid lines above mass histories indicate major mergers, and we show the  $z = 0$  stellar mass ( $M_f^*$  in  $M_\odot$ ) and maximum star-formation rate (in  $M_\odot \text{yr}^{-1}$ ) for each. (a) A galaxy with moderate, fairly constant star-formation rate. (b) A galaxy with some major mergers. By design, the star-formation rate drops to zero immediately following a merger. The star-formation rate recovers within about 2 Gyrs due to gas accretion and possible minor mergers. (c) A galaxy whose major merger quenches almost all subsequent star formation until  $z = 0$ . (d) The complex mass history of the central galaxy in one of the two most massive groups in the simulation. This galaxy undergoes several major mergers, after each of which the SFR recovers within 1 Gyr due to fresh inflows of gaseous fuel.

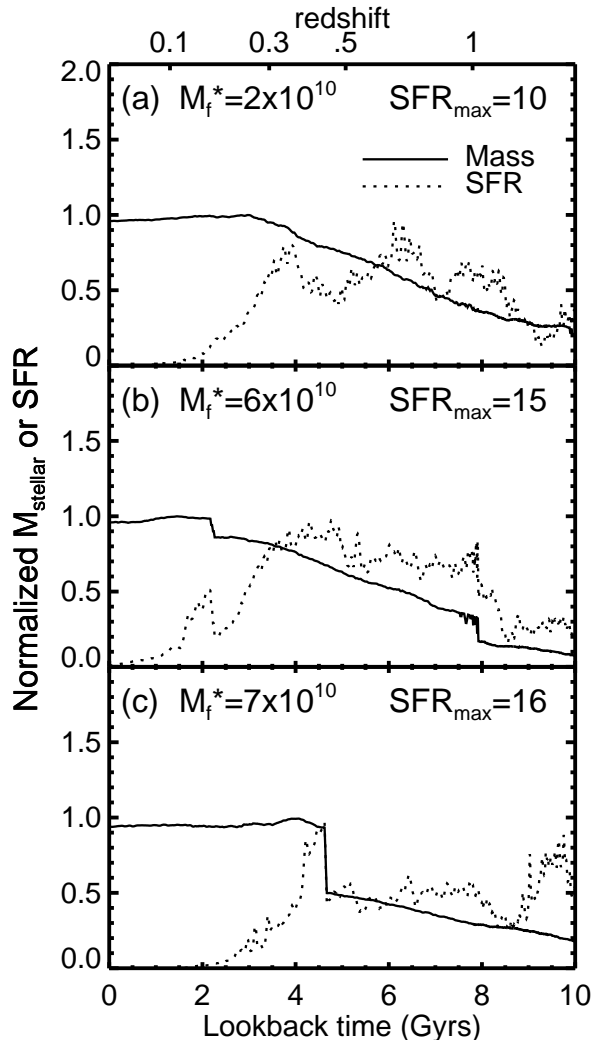


**Figure 7.** Star formation histories (dotted lines) and stellar masses (solid lines) for three galaxies in our hot gas quenching model (cf. Figure 6). (a) A galaxy with fairly quiescent star-formation and steady mass growth. At  $z \approx 0.3$ , this galaxy’s halo becomes dominated by hot gas, after which we begin heating the gas to prevent cooling. Starved of new fuel, star-formation declines to zero over  $\sim 2$  Gyr. (b) A minor merger (lookback time  $\approx 2$  Gyr) delivers fuel to a galaxy which had begun quenching about 2 Gyr earlier. (c) A major merger increases a galaxy’s halo mass to the point where it can support a hot halo, after which it is quenched.

possibly contaminating the red sequence. The observed universe does not contain star-forming galaxies as massive as those shown here, so estimating the extinction in these simulated galaxies would require large extrapolations that are unlikely to be robust. We discuss dust extinction and blue galaxies further in §4.2.

Focusing just on the red sequence, we compare results for models with no quenching, merger quenching, and hot gas quenching in Figure 5. Like the no quenching simulation, the merger quenching model leaves a very sparse red sequence. Our hot gas quenching model, however, produces a red sequence of galaxies well-separated from the blue cloud.

The luminosity function panel in Figure 5 represents

one of the central results of this paper. It emphasizes that our hot gas quenching model nicely produces a sharp truncation in the red galaxy LF, while our merger quenching model does not. Because it produces so few red galaxies, merger quenching does not significantly improve the red galaxy luminosity function of our simulations without quenching. The hot gas quenching model fares well, matching the observed red sequence luminosity function at all magnitudes we resolve.

For the very brightest galaxies, the relatively small volume of our simulations hampers the comparison with data – we do not effectively sample the highest peaks in the density distribution that lead to the most massive galaxies. This is reflected in our errorbars.

Examining the halo quenching red sequence further, we see that it is too blue by about 0.1 magnitudes in  $g - r$ , and has a nearly flat slope that fails to match the observed trend that brighter red galaxies are redder. We examined this issue at length in Gabor et al. (2010), and the same underlying causes are likely here. The overall “blueness problem” may result from either metallicities that are too low or ages that are too young. Our red galaxies have metallicities lower than those inferred for the observed red sequence in the VAGC, and lower metallicities lead to bluer stars. Mean stellar ages of our galaxies are at least as old as those inferred from the observations, so incorrect ages cannot cause the red sequence to be too blue. Since we match the stellar masses, the metallicity deficit is unlikely to owe to an underproduction of stars. It could be that our outflow model ejects too many metals from these systems, or else we might have adopted supernova metal yields that are too low. The red sequence slope poses a subtler problem, perhaps suggesting that simulated massive galaxies merge with too many, too massive, or too young satellite galaxies with lower metallicities. In §4.2, we describe a metallicity re-calibration that matches our simulated red galaxy colors to those observed.

Why does merger quenching fail? In Gabor et al. (2010) we showed that if star formation is completely quenched in the remnants of major mergers, then our models can produce a reasonable match to the red sequence. Merger quenching therefore does not fail because there are too few major mergers. Rather, merger quenching fails because star formation resumes even after a merger remnant loses all its star-forming gas.

We illustrate the resumption of star formation after merging in Figure 6. Each panel corresponds to an individual galaxy taken from a small test simulation with merger quenching. For each galaxy we show the normalized star-formation history (dotted lines) and stellar mass history (solid lines) over cosmic time, with vertical tick marks indicating major mergers. Galaxies with no major mergers (panel a) have fairly constant star formation histories (since  $z \sim 2$ ), with peaks and valleys depending on the details of accretion from the IGM and outflows powered by stars. Galaxies that undergo major mergers (panels b–d) generically stop forming stars when a merger occurs because we instantaneously eject all the cold gas. However, in every case the merger remnant resumes star formation as new fuel is accreted from the IGM. The timing and intensity of the resumption of star-formation varies, probably depending on environment. A very massive galaxy living at the center of a large potential well (panel d) will accrete new gas and re-

turn to high star-formation rates in  $\sim 1$  Gyr. Some smaller galaxies (e.g. panel c) never return to SFRs near their pre-merger levels, though they do resume some star-formation within  $\sim 2$  Gyrs.

As a comparison, we show star-formation histories for quenched galaxies in our hot gas quenching model in Figure 7. The galaxy in panel (a) grows steadily in stellar mass until its halo becomes dominated by hot gas (at  $z \approx 0.3$ ). At this point our hot gas heating cuts off additional fuel for star-formation, and the galaxy gradually uses up its pre-existing reservoir of gas. Star formation peters out after  $\sim 2$  Gyrs. Even after the starvation process begins, merging galaxies can momentarily supply new fuel, as reflected by a jump in SFR in panel (b) at a lookback time of  $\sim 2$  Gyrs. In panel (c) we show a galaxy whose major merger raises its halo mass enough that a hot gas halo becomes stable. These star-formation histories all show a slow decline in star-formation rate over  $\sim 2$  Gyr timescales, similar to the star-formation timescale in our sub-grid star-formation model (Springel & Hernquist 2003). After star formation stops, the galaxy stellar mass declines slowly owing to stellar evolution.

In summary, a simple model where all star formation is quenched in galaxies with a hot halo fraction above 60% produces a red galaxy luminosity function in very good agreement with observations. It also produces a reasonable red sequence, although it is still too blue and too shallow as we saw previously in Gabor et al. (2010), likely reflecting issues with enrichment. In contrast, assuming that all major mergers are associated with  $1500 \text{ km s}^{-1}$  outflows as suggested by observations (Tremonti et al. 2007) does not significantly populate the red sequence.

#### 4.2 Basic models: blue galaxies

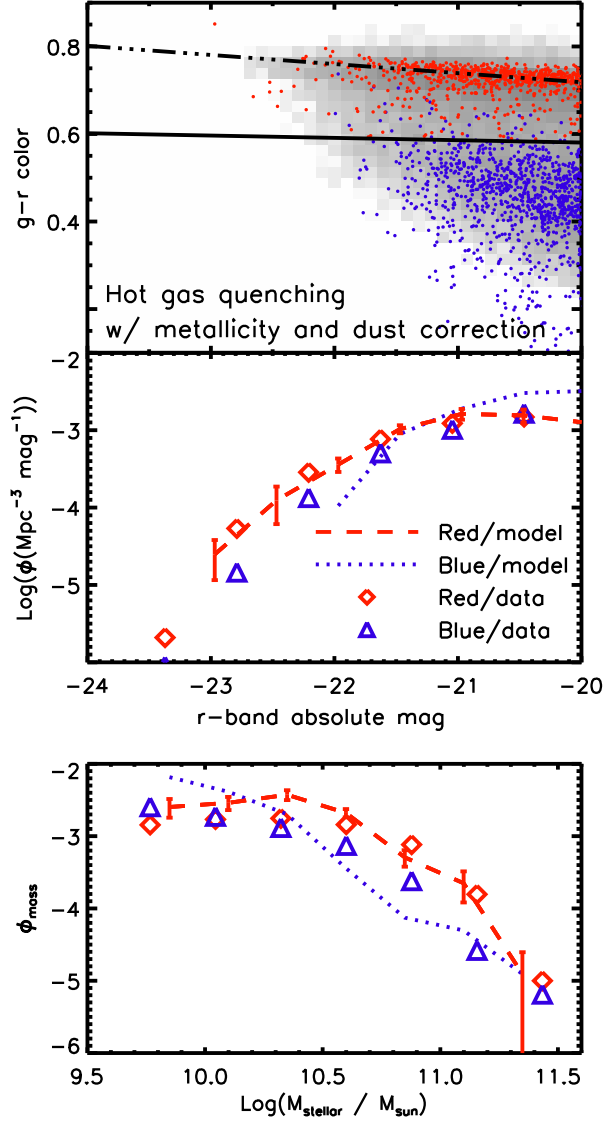
We have shown that additional heating in hot gas halos can produce a red sequence whose luminosity function matches that observed in the local universe. We now examine galaxy colours more closely. Since these are sensitive to uncertain dust corrections and problems with metallicities, we will use galaxy stellar mass functions later in this section.

Figure 8 shows a complete CMD and corresponding LFs for our hot gas quenching model. Here, we apply an ad hoc metallicity correction to force the simulated red sequence to match the observed colors. This assumes that our predicted stellar ages are correct, but that our simulations underpredict stellar metallicities in massive red galaxies. We add a metallicity of  $Z_{\text{add}}$  to each single stellar population (i.e. star particle) when calculating galaxy colors using stellar population synthesis models. By trial and error, we find a good fit using the relation

$$Z_{\text{add}} = 0.003 + (6 \times 10^{-14} M_{\text{stellar}} / M_{\odot}). \quad (2)$$

These are absolute metal mass fractions, and solar metallicity here is  $\approx 0.012$  (Asplund et al. 2005). This correction gives an indication of how far off our metallicities must be. For a  $10^{11} M_{\odot}$  galaxy (with typical absolute magnitude  $r \sim -22$ ),  $Z_{\text{add}} = 0.009$ , representing an increase of  $\sim 50\%$  over typical simulated metallicities for such galaxies.

We show blue galaxies in the CMD with a correction for dust extinction of optical light in the  $g$  and  $r$  bands. In our dust prescription, the  $E(B - V)$  extinction scales with star-formation rate based on empirical relations with



**Figure 8.** Full CMD (top panel), LFs (middle panel), and stellar mass functions (lower panel) for our hot gas quenching model. The simulated CMD includes a metallicity re-scaling to best reproduce the observed red sequence colors, as well as dust reddening and extinction for the blue galaxies. Due to uncertainties in the dust prescription, we prefer to use stellar mass functions (lower panel) to compare simulated and observed blue galaxies. Our hot gas quenching model yields too few massive blue galaxies.

UV luminosity of local galaxies (Wang & Heckman 1996; Somerville et al. 2001; Finlator et al. 2006). We assume a Calzetti et al. (2000) reddening law. This dust prescription yields a blue cloud in fairly good agreement with data, especially in the qualitative shape. It also shifts a small number of intrinsically blue galaxies onto the red sequence, but we count these galaxies as blue for the purposes of calculating the luminosity and mass functions.

In Gabor et al. (2010), we discussed the difficulties in modeling extinction. Given a model galaxy with a specified star-formation and gas accretion history, we need to know the level of dust extinction and reddening to com-

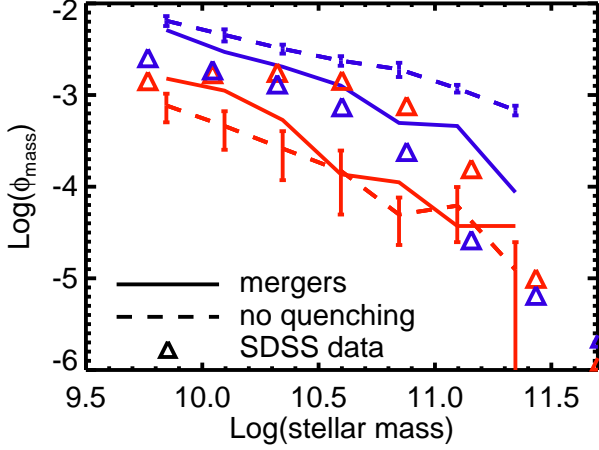


**Figure 9.** Stellar mass functions split into blue and red galaxies (colors) for a simulation with no quenching (dashed lines), a simulation with merger quenching (solid lines), and SDSS data (triangles). Inducing powerful outflows after galaxy mergers does suppress the growth of massive blue galaxies, but it does little to increase the number of red sequence galaxies above that produced in the no-quenching simulation.

pare colors with observed galaxies. Several dust extinction prescriptions keyed to physical properties of galaxies, such as metallicity or star-formation rate, have been proposed (Finlator et al. 2006). Different dust prescriptions yield substantially different colors and magnitudes for our star-forming model galaxies, suggesting large uncertainties. This is especially true for large, bright blue galaxies since these are not well represented in the real Universe. For red galaxies this is not a problem because they have very little extinction (Lauer et al. 2005).

One way to mitigate the large uncertainties in dust obscuration is by examining stellar mass functions for the blue galaxies, rather than luminosity functions. We use stellar mass estimates from Kauffmann et al. (2003b) based on SDSS spectra, which account for extinction self-consistently within the SED fitting procedure for each galaxy. We cross-correlate these stellar mass measurements with galaxies from the VAGC, allowing us to use broad-band colors and generate mass functions using the  $1/V_{\text{max}}$  method. Using the broad-band colors, we separate the galaxies into the red sequence and blue cloud as before.

We show the resulting stellar mass functions for our hot gas quenching model in the bottom panel of Figure 8. As expected from the luminosity function results, and given the tight correspondence between luminosity and mass for old stellar populations, the red galaxy mass function matches the observations well. The blue galaxy stellar mass function is overall a good match to data as well, although it shows a slight underproduction of star-forming galaxies just above the knee of the LF. The small number of galaxies ( $< 10$ ) populating the bright end show only trace levels of star-formation. Our hot fraction criterion ( $f_{\text{hot}} > 60\%$ ) for feedback results in a fairly sharp critical halo mass of  $\sim 10^{12} M_{\odot}$  (Figure 3), and therefore stellar mass of  $\sim 10^{10.5} M_{\odot}$ , above which fueling of star-formation is turned off. Nevertheless, later infall of blue systems can turn a massive galaxy some-

what bluer temporarily. Hence this model produces massive blue galaxies, although the details of that are quite sensitive to our quenching prescription and should be taken with some caution.

This quenching model minimally impacts small galaxies, basically only when they are satellites within larger halos. Davé et al. (2011) show that the fraction of satellite galaxies at these masses is about one-third, which explains why any impact on satellites results in only minor changes to the mass function. At the faint end, our model somewhat overproduces the faint star-forming galaxy population, which is a result also seen in the total mass function examined in Oppenheimer et al. (2010). Thus, while our hot gas quenching model successfully matches the observed number densities of red sequence galaxies, it fails to match all the details of the blue galaxy population.

For comparison, we show the galaxy stellar mass functions for our no-quenching and merger outflows simulations in Figure 9. Solid lines correspond to our no-quenching model, and dashed lines to merger quenching. By ejecting the gas from galaxy merger remnants, we substantially reduce the number density of very massive star-forming galaxies. As indicated by the luminosity function analysis above, merger quenching does not substantially increase the number of red galaxies. In both models, both red and blue mass functions look roughly like power laws, lacking the exponential cutoff observed in SDSS. This shows that merger quenching helps with only one of the two problems in the simulated LFs, namely that it reduces the number of blue galaxies, but it does not increase the number of red galaxies.

In summary, quenching by halo hot fraction successfully reproduces the SDSS red galaxy LF, and broadly reproduces the SDSS red sequence. An empirical augmentation to galaxy metallicities given in equation 2, which increases metal content by typically 50% (with a range of 10–100%), results in an excellent match to the red sequence. The predicted red galaxy mass function is likewise an excellent fit to data, and the blue galaxy mass function broadly matches as well although there is a hint of too few bright galaxies and too many faint ones. The agreement using hot halo quenching is far superior to that using merger quenching, as the latter does not increase the red sequence over a no-quenching model although it does significantly suppress blue galaxies. These simulations therefore suggest that halo gas quenching, by itself, drives the formation of the red sequence.

### 4.3 Model variations

We now consider physically-motivated variations on our basic models. Here we present three variations that all include hot gas heating. In the first we combine our merger winds quenching model with our hot gas heating model. Both of these mechanisms are well-motivated by observations, hence both processes may occur in the real universe. We refer to this as the “combined” model.

In a second variation, we add an exception to the hot gas heating model. Several authors have argued that cold flows of gas along filaments can penetrate hot gas haloes at high redshift, since filaments are denser at earlier epochs. In principle our simulations should capture this behaviour with their hydrodynamic treatment. Our basic hot gas heating model, however, bypasses the hydrodynamics to heat all

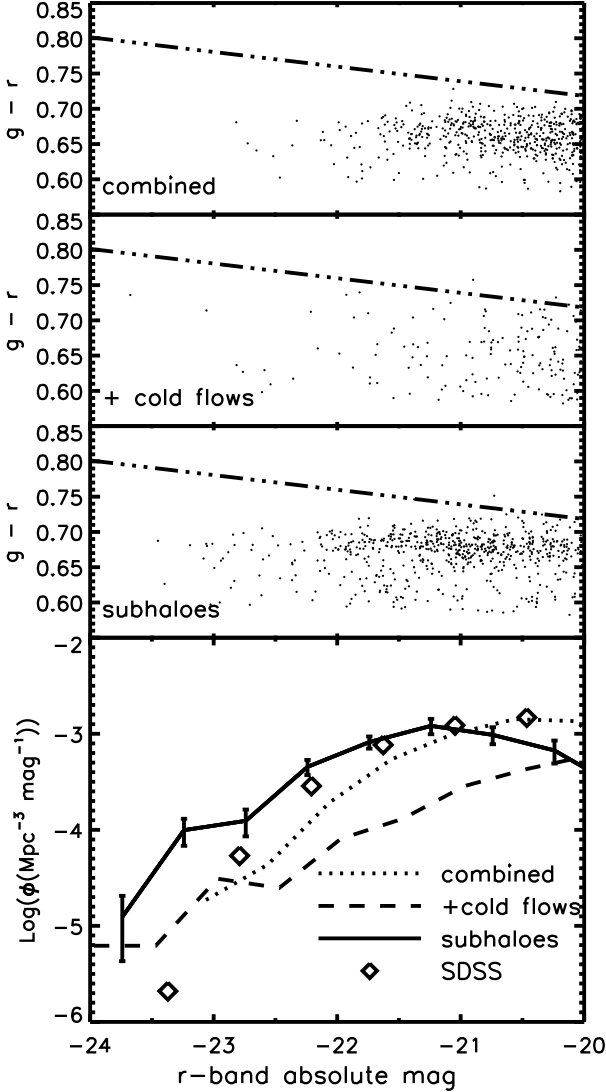


**Figure 10.** CMDs (top 3 panels) and LFs (bottom panel) for three alternative quenching models: combined hot gas heating + merger winds (top CMD, dotted line in LF), the same combined model except *without* heating any gas below 250000 K (middle CMD, dashed line in LF), and a model with hot gas quenching *without* heating gas around sub-haloes (bottom CMD, solid line in LF). The combined model performs well, with slightly lower LFs than the hot gas quenching-only model. Allowing cold flows fails due to wind recycling, and allowing gas fueling in sub-haloes leads to discrepancies at both low and high luminosities in this range.

(non-star-forming) gas around a galaxy. In order to prevent artificial heating of these cold flows, allowing them to penetrate hot haloes, we implemented a model where we only heat gas that is already above our hot gas cutoff of 250000 K. We present this variation with the combined mergers + hot gas model, but we note that the results are similar when we apply this variation to our basic hot gas heating model. We refer to this as the “cold flows” model.

In a third variation, we tested a model where we do not heat the hot gas in the vicinity of sub-haloes. In our simulations, some sub-haloes are embedded in their parent’s hot

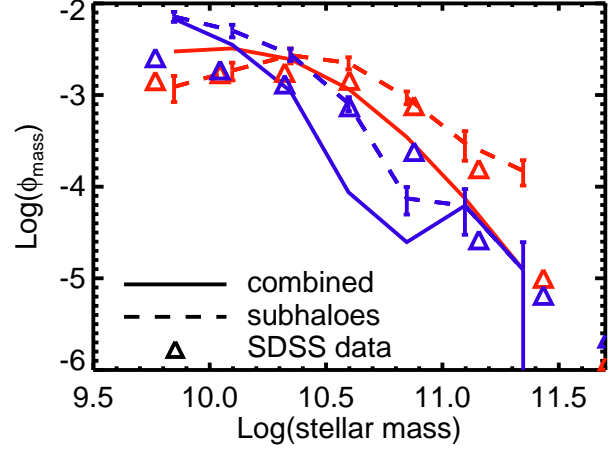


**Figure 11.** Blue and red galaxy mass functions (color-coded) for our combined quenching model (solid lines) and our model without heating gas around sub-haloes (dashed lines). The combined model shows a larger deficit of massive blue galaxies, and the sub-haloes model shows a similar deficit to that in our basic hot gas heating model.

gas halo, even if the sub-halo is too small to support its own hot gas. Our basic quenching model heats the gas in these sub-haloes just the same as in the massive, parent haloes. Heating from AGN feedback is typically observed in the centers of groups and clusters, and it is not clear whether heating from AGN in small satellite galaxies actually occurs in the real Universe. In our simulations, many satellites particularly at low masses are stripped of gas owing to ram pressure or starvation (Davé et al. 2011), but larger satellites are typically star-forming. X-ray observations do suggest that most satellites in clusters have mini cooling cores analogous to those seen in brightest cluster galaxies, and that heating by supernovae or AGN may be necessary to quench them (Sun et al. 2007). Some satellite elliptical galaxies show evidence for AGN outbursts (Jones et al. 2002; Machacek et al. 2006).

To distinguish sub-haloes (or satellite galaxies) from their parent haloes, we use the virial radii estimated when calculating hot gas fractions. If we consider two haloes A and B, then halo A is a subhalo of halo B if and only if (1) the center of halo A falls within halo B’s virial radius and (2) halo B is more massive than halo A. We flag sub-haloes in our group catalog, and we do not add heat to their gas. Note that in this “subhaloes” variant, we do not induce outflows in galaxy merger remnants.

We show results from these three model variations in Figures 10 and 11. Figure 10, analogous to Figure 5, shows CMDs and LFs for just the red sequence in our three variant quenching models. Combined quenching has only a small overall effect on the red sequence when compared to our basic hot gas quenching: at all masses, the number density of red galaxies is slightly below that observed. In short, merger quenching has little overall effect on the galaxy population.

Our “cold flows” model fails to produce a red sequence. This is *not* due primarily to pristine infall along filaments, but rather due to recycling of material expelled by star formation-driven winds (Oppenheimer et al. 2010). Wind

recycling dominates infall in galaxies since  $z \sim 1$ , and is stronger in more massive systems that have short recycling times. Although particles in these systems are ejected at speeds of up to  $\sim 1000$  km/s, their cooling times are short owing to the high level of enrichment, and so many never heat above the shock threshold. We discuss this issue further in §6.

Our variation that excludes heating in sub-haloes (the “subhaloes” model) increases the number of bright red galaxies and decreases the number of faint ( $r \lesssim -20$ ) red ones. The deficit of faint red galaxies is straightforward – turning off quenching in satellites allows those satellites to accrete gas and remain blue. The excess of bright red galaxies arises because the massive galaxies that make up the bright end grow significant mass via mergers with their satellites, even after the central galaxies have been quenched (Gabor et al. 2010). Without quenching, these merging satellites form more stars before they are subsumed than they do with quenching. These mergers then result in more massive central galaxies, and a corresponding increase in the bright-end luminosity function.

To study the blue galaxies in these variant models, we again look at stellar mass functions. Figure 11 shows mass functions for the combined quenching model (solid) and the hot gas quenching model without sub-halo heating. In comparison to our basic hot gas heating model, the combined model results in a sharper cut-off in the blue galaxy mass function above  $M_{\text{stellar}} \sim 10^{10.5} M_{\odot}$ , leading to a larger deficit of massive blue galaxies. The model without sub-halo quenching yields a similar blue galaxy mass function to our basic hot gas heating model.

Overall, the variant models we tested do not solve the underlying problems with our basic models, while introducing new problems. Our combined model exacerbates the deficit of blue galaxies at masses  $\gtrsim 10^{10.5} M_{\odot}$ . Our model with cold flows fails to produce a red sequence. Our model without heating of sub-haloes creates discrepancies in the bright and faint end red galaxy LF.

The combined model leads to similar results as the basic model, but with fewer red sequence galaxies. In Gabor et al. (2010) we showed that the halo mass cutoff, or correspondingly the hot fraction cutoff, above which we quench star-formation largely determines where the exponential cutoff begins in the LF. We therefore expect that raising  $f_{\text{hot}}^{\text{crit}}$  from 0.6 to, say, 0.7 might bring the combined quenching model into better agreement with observations. We cannot therefore easily distinguish between the basic hot gas quenching and the combined quenching models.

In summary, by testing many variants on our basic quenching models, we find that hot gas quenching is required to get a red sequence, while merger quenching has minimal impact. Variations based on not quenching gas in cold flows or subhalos have a noticeable but not large effect on the LF and CMD. None of these variants impact the slope or blueness of the red sequence, which continue to be a difficulty. Hence while all these quenching model variants are physically motivated, in the end a model with simple hot gas quenching matches the ensemble data as well as or better than any of the others.

#### 4.4 The dependence of merger quenching on the critical mass ratio

Studies typically define major mergers as those with a 3:1 mass ratio or smaller. We have adopted this critical mass ratio ( $r = 3$ ) here for merger quenching, assuming that mergers with larger mass ratios have no effect. In this appendix, we show that allowing larger mass ratio mergers to trigger quenching does not lead to a red sequence in better agreement with observations. Although using  $r > 3$  leads, in a general sense, to more quenching, it does not lead to a bimodality in galaxy colors nor a significant number of red galaxies.

Figure 12 compares color-magnitude diagrams and luminosity functions for four different simulations: one with our preferred hot gas quenching model, and our merger quenching model with three values of the critical mass ratio,  $r = 3, 5$ , and 10. These simulations are run with the same resolution as our main simulations, but with a volume  $8\times$  smaller. While this volume does not sample massive galaxies well, it does illustrate the main trends. In particular, we show the hot gas model because it exhibits a well-populated red sequence distinct from the blue cloud. We show marginally resolved galaxies with  $r$ -band  $> -20$  to help clarify the underlying behavior of the simulations.

As described in the text, the merger quenching model under-produces red galaxies while suppressing overall galaxy growth (compared to a model without quenching). This is true for any value of the critical mass ratio. Furthermore, the sparsely populated region of red galaxies is poorly separated from the blue cloud, representing the tail of a unimodal distribution rather than one peak of a bimodal distribution. As we move to higher values of the mass ratio, overall galaxy growth is suppressed more and more, but only a few galaxies at any given time are red. Even with frequent quenching events due to minor mergers, galaxies continuously accrete new material from the IGM to fuel star-formation.

## 5 PHYSICAL IMPACT OF QUENCHING

Our quenching models have many physical and observable implications for galaxies and the IGM. Winds from merger quenching could impact the diffuse IGM. Our hot halo quenching has a major impact because it changes star formation histories. Since outflows associated with star formation enrich the IGM and often end up returning to galaxies, changes in the star-formation rates can lead to changes in IGM and galaxy properties in complicated ways. Exploring all these changes is beyond the scope of this work, but here we explore two physical consequences of quenching – feedback energetics, and the overall build-up of the red sequence.

### 5.1 Quenching energetics

In our simple implementations of quenching mechanisms, we have made no effort to limit the energy available to, e.g., that accreted onto a supermassive black hole. We simply eject or heat up the prescribed gas particles. Here we investigate whether the energy added via quenching is reasonable and in line with expectations.



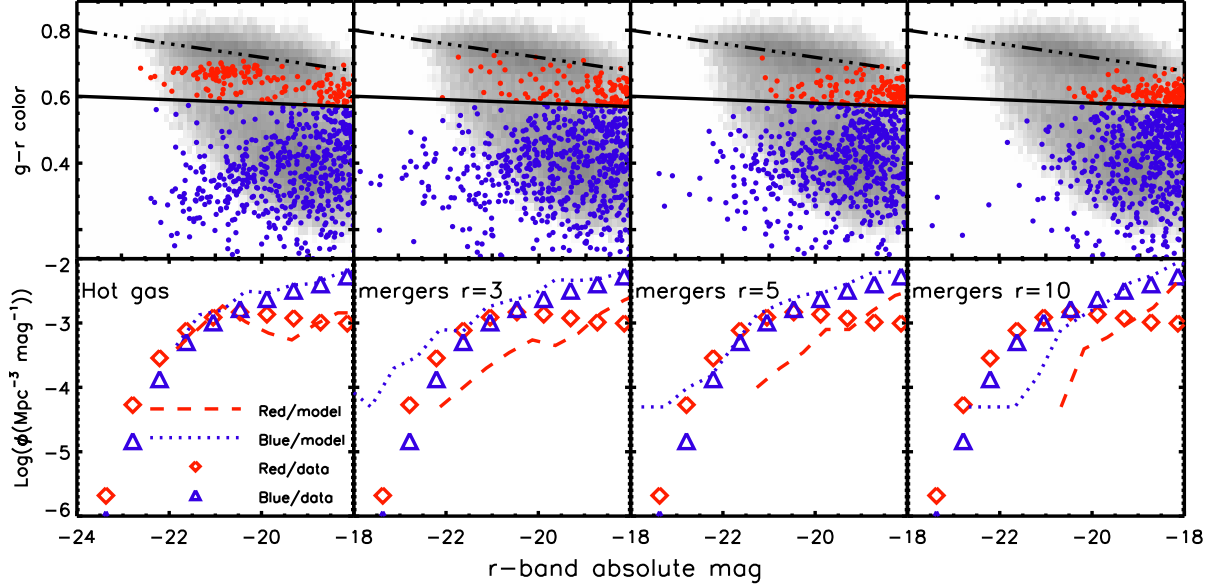


**Figure 12.** Using a critical mass ratio  $r > 3$  to define major mergers does not yield a red sequence, as indicated by colour-magnitude diagrams (top row) and luminosity functions (bottom row) for hot gas quenching (left column) and merger quenching with  $r = 3, 5$ , and  $10$ . These simulations were run in boxes of side length  $24h^{-1}$  Mpc. Even at this smaller volume, hot gas quenching results in an obvious red sequence with number densities close to those observed. Merger quenching with values of  $r > 3$  leads to a stronger suppression of galaxy growth (fewer bright galaxies, e.g. right column), but does not yield a distinct red sequence with substantial number densities.

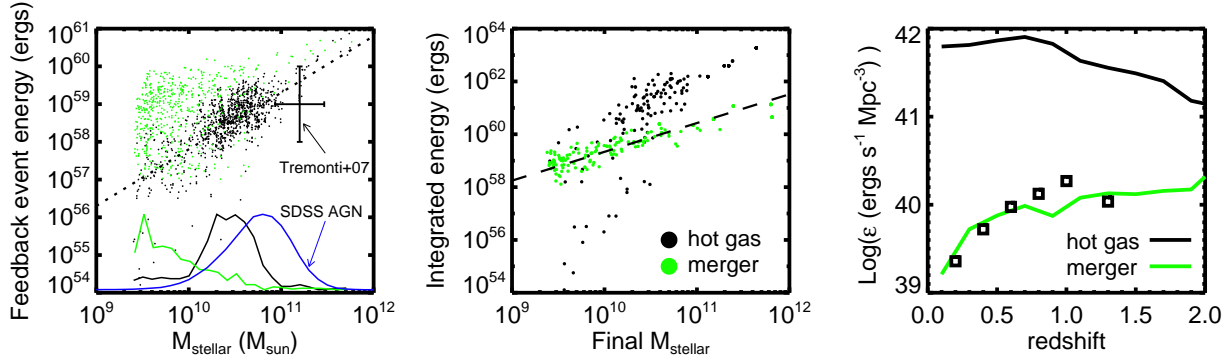


**Figure 13.** Relations between quenching energetics and galaxies, for both merger winds (green) and hot gas heating (black). **Left:** Energy associated with each quenching event vs. the stellar mass of the galaxy hosting that event. Since hot gas heating is actually continuous, each “event” is ambiguous, but corresponds to  $\sim 10^7$  yrs. Errorbars show an estimate of the energy output in winds from post-starburst galaxies based on Tremonti et al. (2007). Corresponding color-coded histograms of stellar mass are shown at the bottom, with blue for optically-selected SDSS AGN. The dotted line shows a scaling  $E \propto M^{2/3}$  motivated by the hydrostatic temperature scaling with halo mass. **Middle:** Time-integrated energy from quenching feedback as a function of  $z = 0$  galaxy stellar mass. This is the total energy of feedback processes over each galaxy’s lifetime, but excludes feedback events that occur in small galaxies that merge with the main progenitor. The dashed line shows the slope of the  $M_{\text{BH}} - M_{\text{stellar}}$  relation for galactic bulges from Bennert et al. (2010). **Right:** Total energy density production rate of feedback processes vs. redshift. Squares show a scaled estimate of the total luminosity density of AGN from Barger et al. (2005).

We track the energy associated with our quenching implementations on galaxy-by-galaxy and event-by-event bases. For hot halo quenching event, we add up the change in energy for each gas particle affected, or quenched, by the event. With hot gas heating, each heated gas particle changes in energy by  $\Delta E = 3/2 N k_B \Delta T = 3/2 (M_{\text{particle}} / (\mu m_p)) k_B \Delta T$ , where  $M_{\text{particle}}$  is the total mass of the particle,  $\mu = 0.6$  is a typical mean molecular weight for gas in clusters (Rosati et al. 2002),  $m_p$  is the

proton mass,  $k_B$  is Boltzmann’s constant, and  $\Delta T$  is the temperature change of the gas particle. Since each heated particle is associated with a galaxy from the group finder, we attribute its change in energy to the feedback energy tally for that galaxy.

In our merger quenching model, we estimate the feedback energy for each particle as the final kinetic energy:  $E = 0.5 M_p v_{\text{kick}}^2$ . Here  $v_{\text{kick}}$  is the kick velocity of gas ejected in winds associated with mergers. The total feedback en-

ergy from a single merger is then summed over all particles that experienced the feedback in a galaxy. Thus, for our basic model, the total energy in a merger is effectively  $E_{\text{merger}} = 0.5M_{\text{coldgas}}(1500\text{kms}^{-1})^2$ , where  $M_{\text{coldgas}}$  is the total cold gas mass in the merger remnant at the time of expulsion.

In Figure 13, we compare our quenching energy calculations to observations associated with feedback processes. In the left panel, we show the energy of each feedback event as a function of its host galaxy’s stellar mass. Since hot gas quenching is actually continuous, there are too many points to plot clearly, so we randomly choose 1000 events. The event energy rises steeply with stellar mass since more massive halos have more gas that requires heating to a higher virial temperature. Since hydrostatic haloes follow the scaling  $M \propto T^{3/2}$ , we overplot a dotted line with  $E \propto M_{\text{stellar}}^{2/3}$  (with arbitrary normalization). The hot gas quenching events follow this trend, although with some scatter, suggesting that the virial temperature is the most important factor in determining how much energy is injected in this model.

Merger quenching shows more scatter and less steep dependence on stellar mass, both of which are driven by gas fraction trends. The event energy for mergers is solely determined by the cold gas mass (since  $v_{\text{kick}}$  is the same for all galaxies), so the scatter in the relation owes to variations in the cold gas mass at any fixed stellar mass. In our simulations, more massive galaxies tend to have smaller gas fractions, which counteracts the overall increase in mass in these systems, leading to a sub-linear relation between merger event energy and host galaxy stellar mass.

For comparison with the merger quenching energetics, we estimate the energy output associated with the massive outflows observed in post-starburst galaxies. Tremonti et al. (2007) measured outflow velocities  $\sim 1000 \text{ km s}^{-1}$ , and estimated outflow masses at  $M_{\text{wind}} \sim 10^{9-11} M_{\odot}$ . From this we estimate the kinetic energy as  $0.5M_{\text{wind}}v_{\text{wind}}^2$ , using the full range of mass estimates to get the errorbars, but neglecting (substantial) variations in wind velocity. Tremonti et al. (2007) also measured stellar masses for their sample of post-starburst galaxies, and we plot errorbars based on the standard deviation of the logarithm of those masses. Our merger outflow energies fall at the high end of this observational estimate, entirely consistent given that we used  $v_{\text{wind}} = 1500 \text{ km s}^{-1}$  in the simulation.

We also show histograms of the stellar mass distribution of feedback events along the  $x$ -axis. As indicated by the black histogram, most hot gas quenching events are associated with galaxy stellar masses between  $10^{10}$  and  $10^{11} M_{\odot}$ . Because of the steep cutoff in the galaxy stellar mass function, there are few galaxies above this mass, and galaxies at lower masses do not have hot halos. In contrast, the distribution of stellar masses of merger events (green line) is skewed toward the low mass end, reflecting the greater frequency of mergers of low-mass galaxies when averaged over cosmic time. For comparison we show in blue the distribution of stellar masses of AGN host galaxies for AGN selected from SDSS using the Baldwin-Phillips-Terlevich (Baldwin et al. 1981) diagnostic with SDSS optical spectra (Kauffmann et al. 2003a). The general trend is similar though the predicted histogram is shifted to somewhat lower masses. This indirectly suggests that AGN activity is indicative of ongoing hot halo quenching.

In the middle panel of Figure 13, we show the time-integrated feedback energy as a function of host galaxy  $z = 0$  stellar mass. If the feedback energy originated from black hole accretion, this enables comparison with final black hole masses, modulo corrections for the efficiency at which accreted mass is converted to output energy, and the coupling of that energy to the gas. As with individual event energies, the integrated energy rises more steeply with stellar mass for hot gas heating than for merger winds. A dashed line shows the slope of the  $M_{\text{BH}} - M_{\text{stellar}}$  relation for local galactic bulges from Bennert et al. (2010), assuming that the integrated feedback energy is  $\propto M_{\text{BH}}$ . The amplitude is arbitrarily normalized to coincide with the mean energy for merger winds at the low-mass end. The slope for merger winds, though slightly shallower than the  $M_{\text{BH}} - M_{\text{stellar}}$  relation, is a good match to the observations. The slope for hot gas quenching is also in good agreement at the high mass end, but drops away quickly to low masses where little energy input has occurred. Note that the observed  $M_{\text{BH}} - M_{\text{stellar}}$  relation uses the *bulge* stellar mass, whereas the simulated galaxies show the total stellar mass. Hence the dropoff to low masses in the hot gas quenching case may partly be reconciled by lower bulge-to-disk ratios in sub- $L^*$  galaxies.

Finally, the right plot shows the energy density production rate of quenching as a function of redshift. This is analogous to the plot of Madau et al. (1998) of galaxy luminosity density evolution, and directly comparable to the plot of Barger et al. (2005) of AGN luminosity density evolution (see also Cowie & Barger 2004). We take data from Figure 25 of Barger et al. for spectroscopically identified sources with  $L_{2-10\text{keV}} \gtrsim 10^{42} \text{ ergs s}^{-1}$  and multiply by their suggested bolometric correction of 35 to get the total luminosity. Then we multiply by a coupling efficiency which determines what fraction of an AGN’s total luminosity couples to the surrounding gas. We choose a somewhat high value of 0.1 (0.05 is typical Di Matteo et al. 2005) to match the normalization of the energy density production rate for the merger quenching model, and show the result as squares in the figure. Outflows from galaxy mergers in our simulations match the shape of measured energetics of luminous AGNs. The total energy requirements for hot gas heating appear much higher. This may indicate that hot gas quenching in the real universe (1) is tied to lower-luminosity AGN, (2) does not heat gas up to the virial temperature, and/or (3) is intermittent with a small duty cycle.

Overall, our results are broadly consistent with the idea that AGN are responsible for providing the energy for quenching feedback. Various authors have already shown that merger-driven feedback can lead to galaxies that are consistent with the  $M - \sigma$  relation; our simulations likewise appear to do so. However, our simulations also show that merger quenching is, in itself, unlikely to be responsible for producing red and dead galaxies. The energetic requirements of hot gas quenching are quite severe in our current model implementation. For instance, such energy injection will excessively heat intragroup gas, likely leading to a mismatch with observed temperature and entropy profiles; we plan to explore this in future work. We speculate that intermittent heating, perhaps triggered by an accumulation of cold gas in the halo center, might work just as well to quench star formation with a significantly lower energy budget. Hence while forcing gas in hot halos to remain at the virial temperature

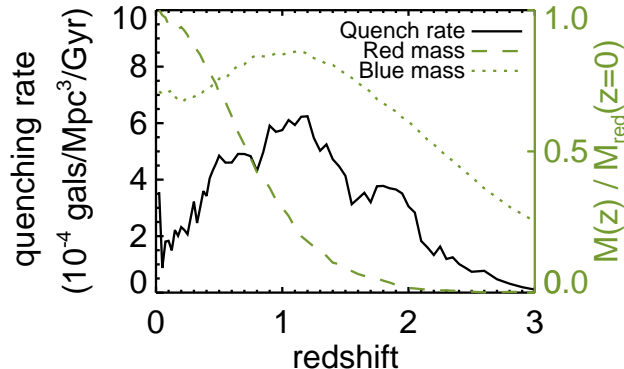


**Figure 14.** Quenching rate (black, left axis) and mass growth history normalized to  $z = 0$  (green, right axis) of red sequence galaxies with  $M_{\text{stellar}} > 10^{9.5} M_{\odot}$  in the hot gas quenching model. In this model, quenching peaks at  $z \approx 1$ , declining at late times. About 2/3 of the mass of the red sequence builds up at  $z < 1$ , while the mass in the blue cloud declines during the same period.

produces a reasonable red galaxy population, further work is required to construct a fully viable physical model.

## 5.2 Red sequence build-up over cosmic time

The build up of the red sequence over time can place strong constraints on quenching physics. Here we investigate two simple parameterizations: the galaxy number quenching rate and the mass growth histories of the red sequence. For both quantities, we restrict ourselves to red galaxies with stellar masses above  $10^{9.5} M_{\odot}$ .

We calculate the quenching rate by comparing each consecutive pair of snapshot outputs from our basic hot gas quenching simulation. The quenching rate,  $dN_{\text{quenched}}/dt$  is estimated as  $\Delta N_{\text{lowssfr}}/\Delta t_{\text{snap}}$ . Here,  $\Delta N_{\text{lowssfr}}$  is the difference in the number of galaxies with specific star formation rates (SSFRs) below  $10^{-12} \text{ yr}^{-1}$  between the two snapshots, and  $\Delta t_{\text{snap}}$  is the time between snapshots. The red sequence mass growth is the total stellar mass in such low-SSFR galaxies,  $M_{\text{red}}(z)$ , normalized to the total stellar mass at in these galaxies  $z = 0$ ,  $M_{\text{red}}(z = 0)$ . We also calculate the mass growth of galaxies with SSFRs above this cutoff,  $M_{\text{blue}}(z)$ , normalizing to the mass in red galaxies  $M_{\text{red}}(z = 0)$  to track relative changes in the blue and red populations.

Figure 14 shows the results. The quenching rate is small at  $z > 2$ , after which it rapidly increases. The rate peaks at  $z \approx 1$ , declining at low redshift. Observations tend to indicate that the mean formation time of stellar populations in massive ellipticals is at  $z \gtrsim 2$  (e.g. Graves et al. 2009). In our model, while massive galaxies tend to have old stellar populations, they do not quench their star formation until typically  $z \sim 1$ . This may be related to why the color-density relation disappears or inverts at  $z \gtrsim 1$ : At low- $z$ , typical central massive galaxies are red, leading to the familiar positive color-density correlation, while prior to  $z \sim 1$  central galaxies have typically not quenched and are blue, leading to an inverted relation.

The total mass on the red sequence at  $z = 1$  is about 1/3 the final value at  $z = 0$ ; half the mass on the present-

day red sequence is in place at  $z = 0.8$ . This significant late build-up is slightly more than the factor of 2 in stellar mass (Bell et al. 2004) and galaxy number (Faber et al. 2007) suggested by observations, although such estimates are presented as lower limits. The mass on the blue cloud rises at early times, declining at  $z < 1$  as many star-forming galaxies become quenched. This reflects a decrease in the number density of blue galaxies by  $\sim 20\%$ , substantially different from the empirical analysis of Blanton (2006), which found no evolution in number density of the observed blue cloud to within 10%. By  $z = 0$ , the total stellar mass in blue galaxies (above our resolution limit of  $\sim 3 \times 10^9 M_{\odot}$ ) is  $\sim 70\%$  that in red galaxies.

## 6 DISCUSSION

### 6.1 Red galaxy morphologies

In this work we have focused on the transformation of galaxy colours, but of course colour and morphology are closely correlated in the local universe. Our simulations' resolution is poorly suited to study morphologies (see e.g. Brook et al. 2011, for a fuller discussion of why). In our favoured hot gas model, starvation by the hot halo only stops star-formation without changing the morphology. Once star-formation stops, a galaxy must undergo (possibly minor) mergers to disrupt the remaining disk and form an elliptical. Such dry (gas-poor) mergers may have difficulty reproducing the observed phase-space densities of stellar orbits in the centres of some elliptical galaxies (Hopkins et al. 2009), but some fraction of the bulge may have built up via dissipational mergers before the galaxy starved (e.g. Bournaud et al. 2007).

One key argument in favor of gas-rich major mergers as a transformative process is that they might turn a star-forming disk into a quiescent elliptical all at once. However, recent observations of quenched late-type galaxies disfavor the merger-only scenario, and suggest that a substantial fraction of passive galaxies must have gone through a “passive disk” phase (Bundy et al. 2010; van der Wel et al. 2010). Our results reinforce the theoretical difficulty seen in earlier models: after halting star-formation at any given time in a galaxy’s evolution, something must prevent future gas accretion to keep that galaxy red and dead (Hopkins et al. 2008; Croton et al. 2006; Bower et al. 2006).

Finally, we note that our hot gas quenching model does not produce passive field galaxies in low-mass haloes (which are not dominated by hot gas), and this may violate observational constraints on the relationship between stellar-mass and the fraction of passive galaxies (Hopkins et al. 2008). Ultimately, morphologies provide an interesting constraint on quenching models, but higher-resolution simulations or sub-resolution morphological models are required to properly apply them. Insofar as galaxy structure influences star-formation histories (Martig et al. 2009), such models may be necessary to understand red galaxy formation.

### 6.2 The importance of hot halo gas

Our favoured model relies on the hot gas surrounding massive galaxies. This hot corona is a robust prediction of years

of theoretical work, yet its existence has not been universally established at mass scales below groups. X-ray observations have revealed diffuse hot gas around only some of the most massive field galaxies (Mulchaey & Jeltema 2010), but recent simulations predict that the halo gas around  $L_{\text{optical}}^*$  galaxies should have X-ray luminosities too faint for current observatories (Crain et al. 2010a). The gas may be there, we just cannot see it.

Why should the hot gas be implicated in shutting down star formation? The hot gas may be crucial to triggering the *type* of feedback that best couples with surrounding gas (i.e. radio jets Di Matteo et al. 2000), or it may simply be a more effective “net” than cold IGM to “catch” the energetic output of an AGN. It seems an unlikely coincidence that the mass scale where a stable hot halo can form just happens to be around the turnover in the stellar mass function, but observations do not unambiguously favor a direct connection. Among field galaxies with diffuse X-ray gas detections, both star-forming and passive galaxies are well-represented (Crain et al. 2010b). This result is not entirely inconsistent with our model – after new accretion is quenched, a galaxy will remain star-forming for  $\sim 2$  Gyrs while surrounded by a substantial hot gaseous halo. Nevertheless, the underabundance of massive star-forming galaxies in our favoured model suggests a less direct relationship between hot gas and quenching than our simple prescription. Perhaps quenching depends jointly on hot gas and the mass of the central black hole, which itself is the product of a complicated history that may involve galaxy mergers and secular growth.

### 6.3 Comparison to other models

Our on-the-fly quenching models build on the post-processing models of Gabor et al. (2010), and the results show some similarities. The color of the red sequence is too blue and roughly constant with mass, which we attribute to difficulties with supernova metal yields, the redistribution of metals by star-formation-driven winds, and/or a poor treatment of merger-induced starbursts in our simulations. We also observe a similar sharp cutoff in the blue galaxy mass function in our best model. A major difference, however, is that re-fueling of merger remnants prevents our merger quenching model from yielding a red sequence, whereas in Gabor et al. (2010) we assumed that all future star-formation was quenched after a merger.

With many successes at matching observations, SAMs also serve as a useful benchmark for our models. Unlike our simulations, typical SAMs already resulted in a substantial red sequence even before invoking quenching feedback models (Croton et al. 2006; Bower et al. 2006). The red galaxies arise due to rapid gas consumption in a starburst associated with a merger or disk instability, or due to gas stripping as a satellite galaxy falls into a larger halo. Our simulations do produce quenched satellites (Davé et al. 2011), but probably do not track secular disk evolution properly. Nevertheless, our merger quenching model shares the generic feature with modern SAMs that further ongoing quenching is required to ensure that the most massive galaxies remain red and dead. Different models incorporate different mechanisms for this added quenching, from various radio mode feedback prescriptions to a simple halo mass cutoff (Croton et al. 2006; Bower et al. 2006; Cattaneo et al.

2006; Somerville et al. 2008). It is worth recognizing that our late-time re-accretion of gas is dominated by recycled winds, something that is not dynamically followed in the SAMs.

Cosmological hydrodynamic simulations akin to ours have included various feedback processes, but (to our knowledge) none has previously produced a realistic red sequence and mass/luminosity function. Simulations with neither stellar nor black hole feedback produce massive galaxies with low star-formation rates, but their stellar masses are much too large (Kereš et al. 2009a). Our simulations with only stellar feedback can bring the low-mass end of the galactic stellar mass function into agreement with observations, but massive galaxies form stars at excessive rates (Oppenheimer et al. 2010). By coupling sub-grid Bondi-Hoyle-Lyttleton black hole accretion with models for the associated energy output, other simulations show promise for matching black hole growth and suppressing star-formation in massive galaxies (Sijacki et al. 2007; Di Matteo et al. 2008; Booth & Schaye 2009, 2010; Degraf et al. 2010; McCarthy et al. 2010), but it is unclear whether they produce a red sequence as observed. Understanding the differences between these models and ours will provide complementary insights into the physical processes behind quenching.

### 6.4 Star-formation driven winds and quenching

Oppenheimer et al. (2010) highlighted the importance of wind recycling accretion in our simulations (without quenching), showing that star-formation in galaxies with  $M_{\text{stellar}} \gtrsim 10^{10} M_{\odot}$  is fueled mainly by gas that was earlier ejected in winds. Because this wind recycling dominates the fuel for star-formation in massive galaxies, it is the main fueling mode we are trying to quench in this work.

Our treatment of star-formation driven winds may not be physically accurate. Once launched, we decouple the winds from hydrodynamic interactions with surrounding gas to allow them to escape the galaxy in a resolution-converged way (Springel & Hernquist 2003; Schaye et al. 2010). Even after re-activation of the hydrodynamics, the wind particles may not merge seamlessly with surrounding gas. Upon escape from galaxies, wind particles are cold, dense, and metal-rich. While they decrease in density as they move away from the galaxy, they remain enriched since we don’t include diffusion of metals among gas particles. Metal-line cooling makes them cool faster than surrounding gas, so they stay cold and dense, and more likely to return to galaxies. It is unclear how realistic the assumed complete lack of mixing is, but we note that this wind model has resulted in agreement with observations of IGM metal absorbers (Oppenheimer & Davé 2006, 2008; Oppenheimer et al. 2009).

Wind recycling, and the possibility of over-recycling, has implications for all our quenching models. As shown in Oppenheimer et al. (2010) and Gabor et al. (2010), simply stopping wind recycling is unlikely to produce a realistic red sequence – doing so suppresses star formation too much to create enough  $\sim L^*$  galaxies, while small amounts of cold and hot accretion keep too many galaxies forming stars. In our merger quenching model, we have emphasized the re-fueling of merger remnants after  $\sim 2$  Gyr. Based on the origin of star-forming gas explored in Oppenheimer et al.

(2010), most of the accreted fuel comes from wind recycling, although a significant sub-dominant component comes from cold and hot accretion. Therefore in our hot gas quenching model, where we expressly heat all non-star-forming gas, most of the gas we must quench had been expelled in winds. Hence we caution that the hydrodynamics of winds may play a critical role in quantitatively assessing the amount and location of quenching feedback needed to produce a red sequence.

## 6.5 Guidelines for future models

Given the wide range of physical scales important in galaxy evolution, developers of cosmological simulations have little choice but to resort to sub-resolution quenching models for the foreseeable future. Here we discuss ways of improving these models. Any model quenching mechanism requires 3 steps:

- (i) Criteria to start (and stop) the feedback process.
- (ii) An estimate of the energy budget or luminosity available.
- (iii) A method to couple feedback energy to surrounding gas.

The first two steps may be linked in models where the feedback energy varies over time: e.g. the black hole accretion rate varies by several orders of magnitude between states where the feedback is important and negligible. In our current hot gas quenching model, (i) is the existence of a hot gas-dominated halo, (ii) is effectively unlimited, and for (iii) we heat all the non-star-forming gas in the FOF group. We have seen that this successfully creates a red sequence of galaxies, but that it leads to a dearth of star-forming galaxies with  $M_{\text{stellar}} \gtrsim 10^{10.5} M_{\odot}$  and requires too much energy input. Below we discuss each of these steps in the context of radio mode AGN feedback.

### 6.5.1 (i) Triggering mechanisms

Triggering radio mode feedback requires accretion onto a supermassive black hole. In massive (cluster) haloes, the black hole may accrete directly from the hot halo in a Bondi process (Quataert & Narayan 2000), or a black hole may be fueled by cold clouds that condense from the hot medium (Soker 2006; McNamara et al. 2010). Bondi accretion of hot gas may be more conducive to the formation of a powerful radio jet than rapid, radiatively efficient accretion (Di Matteo et al. 2000). The formation of a jet may additionally require significant black hole spin (Narayan & Quataert 2005). Based on the present work, the presence of hot gas seems to be crucial for triggering radio mode feedback.

Models have used a variety of triggers for AGN feedback. SAMs typically assume that feedback operates in hot, massive haloes. Hydrodynamic models usually adopt a Bondi-Hoyle prescription, or a simple scaling with gas mass in the black hole vicinity (Vernaleo & Reynolds 2006; Brüggen & Scannapieco 2009), to control black hole accretion and thus triggering.

Observationally, most X-ray bright clusters, groups, and elliptical galaxies host some level of central radio AGN, with

AGN more likely in systems with shorter central cooling times, and more luminous in more massive systems (Burns 1990; Mittal et al. 2009; Sun 2009; Dunn et al. 2010). Outbursts that induce X-ray cavities typically occur every  $10^{7-8}$  years with energies  $\sim 10^{55-60}$  ergs (Voit & Donahue 2005; David et al. 2010; Randall et al. 2010). These observations suggest a triggering mechanism linked to gas cooling in the central regions of a hot halo, which may be a resolvable triggering mechanism in cosmological simulations. This may provide a more observationally-calibratable method for triggering AGN feedback than Bondi-Hoyle accretion.

### 6.5.2 (ii) Available energy for feedback

The energy of feedback mainly depends on the black hole accretion rate. Most models assume some fraction of the accretion rest-mass-energy acts on surrounding gas. The accretion rate is typically determined through simple scalings with black hole and halo mass in SAMs and through Bondi-Hoyle models in simulations.

Observations suggest kinetic power output from central bursts of  $\sim 10^{45} \text{ erg s}^{-1}$  over  $\sim 10^8$  years in some clusters, consistent with total energy in inflated bubbles ( $\sim 10^{60}$  ergs). As mentioned above, radio emission scales with cluster size, but it is not clear to what extent the burst energies depend on halo properties. The fact that few very massive galaxies have enough star-formation to give them blue colors suggests that there is enough heating power to offset cooling. This may imply a self-regulating cycle (cf. Ciotti & Ostriker 1997, 2001; Churazov et al. 2005). Hydrodynamic models that directly track black hole accretion or use some estimate based on the mass within the central regions of the halo can achieve this self-regulation (e.g. Brüggen & Scannapieco 2009).

In our hot gas quenching model, the required energy budget is large, although it is not clear that significantly less energy input could be equally effective. It is also difficult to exceed the theoretical maximum energy output of black holes; models typically assume efficiency of mass-energy coupling to surrounding gas of less than 1%. So the energy budget remains an interesting constraint, but the most attractive scenario is that black holes emit just enough energy to remove or starve their cold gas reservoir, at which point they become quiescent again.

### 6.5.3 (iii) Coupling of feedback to gas

How AGN energy couples with the surrounding medium is another matter of debate. Supersonic jets induce bow shocks in the surrounding gas (Voit & Donahue 2005; Randall et al. 2010), and subsonic jets entrain material and thermalize their energy via turbulent mixing (De Young 2010). The outflows can apparently evacuate  $\sim 10$  kpc-scale “bubbles” in hot intragroup gas (Birzan et al. 2004), and the bubbles then share their energy at scales  $\sim 10 - 100$  kpc via buoyant uplift, mixing, and sound waves (Churazov et al. 2001; Voit & Donahue 2005; Nulsen et al. 2007; Scannapieco & Brüggen 2008; Brüggen & Scannapieco 2009; Fabian et al. 2003; Sanders & Fabian 2007, 2008).

While idealized hydrodynamic models have directly

examined the interaction of jets and bubbles with the ICM (e.g. Ruszkowski et al. 2004; Brüggen et al. 2005; Heinz et al. 2006; Scannapieco & Brüggen 2008; Brüggen et al. 2009; Morsony et al. 2010; Mendygral et al. 2011), SAMs typically assume that feedback directly offsets the cooling for simplicity. Cosmological hydrodynamic simulations usually inject the feedback energy into one or a few resolution elements near the black hole, relying on the hydrodynamic calculations to distribute the energy to large scales in the halo (e.g. Booth & Schaye 2009; Teyssier et al. 2011). In our models, suppressing star-formation in accordance with observations requires heating gas throughout the circum-galactic region, on scales of  $> 10$  kpc, to prevent the formation of cold clumps.

In summary, a path for modeling quenching feedback would be as follows: 1) Trigger feedback when the central cooling time drops below e.g. 1 Gyr, or some fraction of the hubble time; 2) Calculate energy for feedback as some fraction of the rest-mass energy of cold or cooling gas in the central regions; 3) Increase the entropy of the gas with some radial dependence in a manner consistent with higher-resolution simulations. We will explore models based on these principles in future work.

## 7 SUMMARY AND CONCLUSION

With the goal of building a realistic red sequence of galaxies in cosmological hydrodynamic simulations, we have implemented novel mechanisms for quenching star-formation in the simulation code GADGET-2. By identifying mergers and halos on-the-fly within simulations, we implement and test various models for quenching feedback related to these processes. While our work is motivated by feedback resulting from AGN, we explicitly avoid examining black hole growth in order to concentrate on constraints from the massive galaxy population.

Motivated by observations of massive outflows from post-starburst galaxies attributed to quasar feedback, we implement  $1500 \text{ km s}^{-1}$  superwinds in the remnants of galaxy mergers that expels all the cold gas. To do so, we first use an FOF group finder to identify galaxy mergers on-the-fly, and then give a velocity kick to all the star-forming gas. We have shown that this quenching mechanism alone does not produce a red sequence in our simulations. Even after all the gas is expelled from a merger remnant, new supplies of gas accrete from the IGM to re-fuel star-formation, typically within  $\sim 2$  Gyr.

Motivated by observations of radio AGN and X-ray cavities in the hot gas of galaxy groups, we add thermal heating to hot gas in massive dark matter haloes. We calculate the hot gas fraction  $f_{\text{hot}}$  in the halo, and if  $f_{\text{hot}} > 0.6$  (roughly corresponding to halo masses  $\gtrsim 10^{12} M_{\odot}$ ), then we heat all its gas outside of the ISM to the halo virial temperature. By keeping the surrounding gas hot, we starve galaxies embedded in hot haloes of new fuel for star-formation. We have shown that this hot gas quenching model yields a red sequence whose luminosity function provides an excellent match with observations of local galaxies (Figure 5).

Our main results are:

- Galactic-scale outflows triggered by mergers (i.e. quasar mode feedback) do not produce a substantial red sequence

on their own because gas accretion from the IGM re-fuels star-formation within  $\sim 1 - 2$  Gyr.

- Adding thermal energy to hot X-ray gas around massive galaxies (analogous to radio mode AGN feedback) successfully produces a red sequence whose luminosity function matches observations.

- This heating must occur around satellite galaxies embedded in the hot gas of their parent haloes to match the faint-end red galaxy luminosity function.

- A combination of hot gas heating with merger-triggered outflows may be empirically motivated and perform as well as the heating-only model, but hot gas heating is the crucial required component.

- Our simple hot gas heating model produces somewhat too few massive blue galaxies, possibly owing to the sharp truncation in gas accretion onto galaxies as soon as their haloes are dominated by hot gas.

- As in Gabor et al. (2010), our baseline model produces a red sequence that is too blue and too shallow, likely owing to issues related to enrichment. We empirically recalibrate the metallicities to obtain agreement, which requires a metallicity increase up to  $\times 2$  in the most massive systems.

The overall success of reproducing the observed red sequence and associated luminosity function is a first for cosmological hydrodynamic simulations. Doing so has already elucidated stringent constraints on how quenching must operate under the scenarios explored. While hot halo quenching appears to be necessary and sufficient to reproduce observations of red galaxies as well as any model at  $z = 0$ , our current simplistic implementation requires more energy than is thought to be available and likely overheats surrounding gas. We have yet to explore details of redshift evolution, clustering, or the impact of quenching on the surrounding intergalactic gas; these may motivate variants on this simple scenario. The beauty of implementing quenching models self-consistently within large-scale hydrodynamics simulations of galaxy formation is that such models open up a host of new avenues to constrain quenching physics.

In future work, we aim to develop more physically consistent models for quenching star-formation. To do so, we advocate connecting well-resolved structures and processes in the simulations to feedback processes that operate below the resolution scale. Such sub-resolution models will require guidance from observations and higher-resolution simulations of individual galaxies or clusters. We outline a particular path forward for this based on current intuition that we will explore in future work. By combining insights from advancing theoretical work on all scales and advancing observations across cosmic time, we hope to continue refining our models to better understand how massive red and dead galaxies come to be.

## ACKNOWLEDGMENTS

The authors acknowledge N. Katz, D. Keres, J. Kollmeier, A. van der Wel, and D. Weinberg for helpful discussions, the referee for useful comments, and V. Springel for making Gadget-2 public. The simulations used here were run on University of Arizona's SGI cluster, ice. This work was supported by the National Science Foundation under grant



numbers AST-0847667 and AST- 0907998. Computing resources were obtained through grant number DMS-0619881 from the National Science Foundation. KF acknowledges support from NASA through Hubble Fellowship grant HF-51254.01 awarded by the Space Telescope Science Institute, which is operated by the Association of Universities for Research in Astronomy, Inc., for NASA, under contract NAS 5-26555.

## REFERENCES

- Adelman-McCarthy J. K. et al., 2008, *ApJS*, 175, 297
- Asplund M., Grevesse N., Sauval A. J., 2005, in *Astronomical Society of the Pacific Conference Series*, Vol. 336, *Cosmic Abundances as Records of Stellar Evolution and Nucleosynthesis*, T. G. Barnes III & F. N. Bash, ed., pp. 25–+
- Bahcall J. N., Kirhakos S., Saxe D. H., Schneider D. P., 1997, *ApJ*, 479, 642
- Baldry I. K., Glazebrook K., Brinkmann J., Ivezić Ž., Lup-ton R. H., Nichol R. C., Szalay A. S., 2004, *ApJ*, 600, 681
- Baldwin J. A., Phillips M. M., Terlevich R., 1981, *PASP*, 93, 5
- Balogh M. L., Baldry I. K., Nichol R., Miller C., Bower R., Glazebrook K., 2004, *ApJ*, 615, L101
- Barger A. J., Cowie L. L., Mushotzky R. F., Yang Y., Wang W., Steffen A. T., Capak P., 2005, *AJ*, 129, 578
- Barnes J. E., Hernquist L., 1992, *ARA&A*, 30, 705
- Bauer F. E., Fabian A. C., Sanders J. S., Allen S. W., Johnstone R. M., 2005, *MNRAS*, 359, 1481
- Bell E. F. et al., 2004, *ApJ*, 608, 752
- Bennert N., Canalizo G., Jungwiert B., Stockton A., Schweizer F., Peng C. Y., Lacy M., 2008, *ApJ*, 677, 846
- Bennert V. N., Auger M. W., Treu T., Woo J., Malkan M. A., 2010, *ArXiv e-prints*
- Best P. N., Kaiser C. R., Heckman T. M., Kauffmann G., 2006, *MNRAS*, 368, L67
- Birnboim Y., Dekel A., 2003, *MNRAS*, 345, 349
- , 2010, *ArXiv e-prints*
- Birnboim Y., Dekel A., Neistein E., 2007, *MNRAS*, 380, 339
- Birzan L., Rafferty D. A., McNamara B. R., Wise M. W., Nulsen P. E. J., 2004, *ApJ*, 607, 800
- Blanton M. R., 2006, *ApJ*, 648, 268
- Blanton M. R. et al., 2005, *AJ*, 129, 2562
- Booth C. M., Schaye J., 2009, *MNRAS*, 398, 53
- , 2010, *MNRAS*, 405, L1
- Bournaud F., Jog C. J., Combes F., 2007, *A&A*, 476, 1179
- Bower R. G., Benson A. J., Malbon R., Helly J. C., Frenk C. S., Baugh C. M., Cole S., Lacey C. G., 2006, *MNRAS*, 370, 645
- Brook C. B. et al., 2011, *MNRAS*, 595
- Brüggen M., Ruzsowski M., Hallman E., 2005, *ApJ*, 630, 740
- Brüggen M., Scannapieco E., 2009, *MNRAS*, 398, 548
- Brüggen M., Scannapieco E., Heinz S., 2009, *MNRAS*, 395, 2210
- Bruzual G., Charlot S., 2003, *MNRAS*, 344, 1000
- Bundy K. et al., 2010, *ApJ*, 719, 1969
- Burns J. O., 1990, *AJ*, 99, 14
- Calzetti D., Armus L., Bohlin R. C., Kinney A. L., Koornneef J., Storchi-Bergmann T., 2000, *ApJ*, 533, 682
- Canalizo G., Stockton A., 2001, *ApJ*, 555, 719
- Cattaneo A., Dekel A., Devriendt J., Guiderdoni B., Blaizot J., 2006, *MNRAS*, 370, 1651
- Churazov E., Brüggen M., Kaiser C. R., Böhringer H., Forman W., 2001, *ApJ*, 554, 261
- Churazov E., Sazonov S., Sunyaev R., Forman W., Jones C., Böhringer H., 2005, *MNRAS*, 363, L91
- Ciotti L., Ostriker J. P., 1997, *ApJ*, 487, L105+
- , 2001, *ApJ*, 551, 131
- Cisternas M. et al., 2011, *ApJ*, 726, 57
- Cowie L. L., Barger A. J., 2004, in *Astrophysics and Space Science Library*, Vol. 308, *Supermassive Black Holes in the Distant Universe*, A. J. Barger, ed., pp. 273–+
- Crain R. A., McCarthy I. G., Frenk C. S., Theuns T., Schaye J., 2010a, *MNRAS*, 407, 1403
- Crain R. A., McCarthy I. G., Schaye J., Frenk C. S., Theuns T., 2010b, *ArXiv e-prints*
- Crawford C. S., Allen S. W., Ebeling H., Edge A. C., Fabian A. C., 1999, *MNRAS*, 306, 857
- Croton D. J. et al., 2006, *MNRAS*, 365, 11
- Davé R., Finlator K., Oppenheimer B. D., 2006, *MNRAS*, 370, 273
- , 2007, in *EAS Publications Series*, Vol. 24, *EAS Publications Series*, E. Emsellem, H. Wozniak, G. Massacrier, J.-F. Gonzalez, J. Devriendt, & N. Champavert, ed., pp. 183–189
- Davé R., Oppenheimer B. D., Finlator K., 2011, *ArXiv e-prints*
- David L. P. et al., 2010, *ArXiv e-prints*
- De Lucia G., Boylan-Kolchin M., Benson A. J., Fontanot F., Monaco P., 2010, *MNRAS*, 406, 1533
- De Young D. S., 2010, *ApJ*, 710, 743
- DeBuhr J., Quataert E., Ma C., 2010, *ArXiv e-prints*
- DeBuhr J., Quataert E., Ma C., Hopkins P., 2009, *ArXiv e-prints*
- Degraf C., Di Matteo T., Springel V., 2010, *MNRAS*, 402, 1927
- Dekel A., Birnboim Y., 2006, *MNRAS*, 368, 2
- , 2008, *MNRAS*, 383, 119
- Dekel A., Birnboim Y., Engel G., Freundlich J., Goerdt T., Mumcuoglu M., Neistein E., Pichon C., Teyssier R., Zinger E., 2009a, *Nature*, 457, 451
- Dekel A., Sari R., Ceverino D., 2009b, *ApJ*, 703, 785
- Di Matteo T., Colberg J., Springel V., Hernquist L., Sijacki D., 2008, *ApJ*, 676, 33
- Di Matteo T., Quataert E., Allen S. W., Narayan R., Fabian A. C., 2000, *MNRAS*, 311, 507
- Di Matteo T., Springel V., Hernquist L., 2005, *Nature*, 433, 604
- Donahue M. et al., 2010, *ApJ*, 715, 881
- Donahue M., Horner D. J., Cavagnolo K. W., Voit G. M., 2006, *ApJ*, 643, 730
- Dunn R. J. H., Allen S. W., Taylor G. B., Shurkin K. F., Gentile G., Fabian A. C., Reynolds C. S., 2010, *MNRAS*, 404, 180
- Eggen O. J., Lynden-Bell D., Sandage A. R., 1962, *ApJ*, 136, 748
- Faber S. M. et al., 2007, *ApJ*, 665, 265
- Fabian A. C., 1994, *ARA&A*, 32, 277
- Fabian A. C., Nulsen P. E. J., Canizares C. R., 1984, *Na-*

- ture, 310, 733
- Fabian A. C., Sanders J. S., Allen S. W., Crawford C. S., Iwasawa K., Johnstone R. M., Schmidt R. W., Taylor G. B., 2003, *MNRAS*, 344, L43
- Fabian A. C. et al., 2000, *MNRAS*, 318, L65
- Fabian A. C., Sanders J. S., Taylor G. B., Allen S. W., Crawford C. S., Johnstone R. M., Iwasawa K., 2006, *MNRAS*, 366, 417
- Feruglio C., Maiolino R., Piconcelli E., Menci N., Aussel H., Lamastra A., Fiore F., 2010, *ArXiv e-prints*
- Finlator K., Davé R., 2008, *MNRAS*, 385, 2181
- Finlator K., Davé R., Oppenheimer B. D., 2007, *MNRAS*, 376, 1861
- Finlator K., Davé R., Papovich C., Hernquist L., 2006, *ApJ*, 639, 672
- Gabor J. M., Davé R., Finlator K., Oppenheimer B. D., 2010, *MNRAS*, 407, 749
- Gabor J. M. et al., 2009, *ApJ*, 691, 705
- Georgakakis A. et al., 2009, *MNRAS*, 397, 623
- Giodini S. et al., 2010, *ApJ*, 714, 218
- Graves G. J., Faber S. M., Schiavon R. P., 2009, *ApJ*, 693, 486
- Grogin N. A. et al., 2005, *ApJ*, 627, L97
- Guo F., Oh S. P., 2008, *MNRAS*, 384, 251
- Heinz S., Brüggen M., Young A., Levesque E., 2006, *MNRAS*, 373, L65
- Hernquist L., 1989, *Nature*, 340, 687
- Hicks A. K., Mushotzky R., 2005, *ApJ*, 635, L9
- Hopkins P. F., Cox T. J., Dutta S. N., Hernquist L., Kormendy J., Lauer T. R., 2009, *ApJS*, 181, 135
- Hopkins P. F., Cox T. J., Kereš D., Hernquist L., 2008, *ApJS*, 175, 390
- Hutchings J. B., Johnson I., Pyke R., 1988, *ApJS*, 66, 361
- Johansson P. H., Naab T., Ostriker J. P., 2009, *ApJ*, 697, L38
- Jones C., Forman W., Vikhlinin A., Markevitch M., David L., Warmflash A., Murray S., Nulsen P. E. J., 2002, *ApJ*, 567, L115
- Jubelgas M., Springel V., Dolag K., 2004, *MNRAS*, 351, 423
- Kauffmann G., Heckman T. M., Tremonti C., Brinchmann J., Charlot S., White S. D. M., Ridgway S. E., Brinkmann J., Fukugita M., Hall P. B., Ivezić Ž., Richards G. T., Schneider D. P., 2003a, *MNRAS*, 346, 1055
- Kauffmann G., Heckman T. M., White S. D. M., Charlot S., Tremonti C., Brinchmann J., Bruzual G., Peng E. W., Seibert M., Bernardi M., Blanton M., Brinkmann J., Castander F., Csábai I., Fukugita M., Ivezić Z., Munn J. A., Nichol R. C., Padmanabhan N., Thakar A. R., Weinberg D. H., York D., 2003b, *MNRAS*, 341, 33
- Kennicutt Jr. R. C., 1998, *ApJ*, 498, 541
- Kereš D., Katz N., Davé R., Fardal M., Weinberg D. H., 2009a, *MNRAS*, 396, 2332
- Kereš D., Katz N., Fardal M., Davé R., Weinberg D. H., 2009b, *MNRAS*, 395, 160
- Kereš D., Katz N., Weinberg D. H., Davé R., 2005, *MNRAS*, 363, 2
- Khochfar S., Ostriker J. P., 2008, *ApJ*, 680, 54
- Komatsu E. et al., 2009, *ApJS*, 180, 330
- Lauer T. R. et al., 2005, *AJ*, 129, 2138
- Levine R., Gnedin N. Y., Hamilton A. J. S., 2010, *ApJ*, 716, 1386
- Lu Y., Kereš D., Katz N., Mo H. J., Fardal M., Weinberg M. D., 2010, *ArXiv e-prints*
- Machacek M., Nulsen P. E. J., Jones C., Forman W. R., 2006, *ApJ*, 648, 947
- Madau P., Pozzetti L., Dickinson M., 1998, *ApJ*, 498, 106
- Maller A. H., Katz N., Kereš D., Davé R., Weinberg D. H., 2006, *ApJ*, 647, 763
- Martig M., Bournaud F., Teyssier R., Dekel A., 2009, *ApJ*, 707, 250
- Martin C. L., 2005, *ApJ*, 621, 227
- McCarthy I. G. et al., 2010, *MNRAS*, 406, 822
- McKee C. F., Ostriker J. P., 1977, *ApJ*, 218, 148
- McLure R. J., Kukula M. J., Dunlop J. S., Baum S. A., O’Dea C. P., Hughes D. H., 1999, *MNRAS*, 308, 377
- McNamara B. R., Nulsen P. E. J., Wise M. W., Rafferty D. A., Carilli C., Sarazin C. L., Blanton E. L., 2005, *Nature*, 433, 45
- McNamara B. R. et al., 2006, *ApJ*, 648, 164
- McNamara B. R., Rohanizadegan M., Nulsen P. E. J., 2010, *ArXiv e-prints*
- McNamara B. R. et al., 2000, *ApJ*, 534, L135
- Mendygral P. J., O’Neill S. M., Jones T. W., 2011, *ApJ*, 730, 100
- Mittal R., Hudson D. S., Reiprich T. H., Clarke T., 2009, *A&A*, 501, 835
- Morsony B. J., Heinz S., Brüggen M., Ruszkowski M., 2010, *MNRAS*, 407, 1277
- Mulchaey J. S., Jeltama T. E., 2010, *ApJ*, 715, L1
- Murray N., Quataert E., Thompson T. A., 2005, *ApJ*, 618, 569
- Narayan R., Quataert E., 2005, *Science*, 307, 77
- Nulsen P. E. J., Jones C., Forman W. R., David L. P., McNamara B. R., Rafferty D. A., Bîrzan L., Wise M. W., 2007, in *Heating versus Cooling in Galaxies and Clusters of Galaxies*, H. Böhringer, G. W. Pratt, A. Finoguenov, & P. Schuecker, ed., pp. 210–+
- Ocvirk P., Pichon C., Teyssier R., 2008, *MNRAS*, 390, 1326
- Oppenheimer B. D., Davé R., 2006, *MNRAS*, 373, 1265
- , 2008, *MNRAS*, 387, 577
- Oppenheimer B. D., Davé R., Finlator K., 2009, *MNRAS*, 396, 729
- Oppenheimer B. D., Davé R., Kereš D., Fardal M., Katz N., Kollmeier J. A., Weinberg D. H., 2010, *MNRAS*, 406, 2325
- Padmanabhan N. et al., 2008, *ApJ*, 674, 1217
- Parrish I. J., Quataert E., Sharma P., 2009, *ApJ*, 703, 96
- Quataert E., Narayan R., 2000, *ApJ*, 528, 236
- Quillen A. C. et al., 2008, *ApJS*, 176, 39
- Randall S. W. et al., 2010, *ArXiv e-prints*
- Rees M. J., Ostriker J. P., 1977, *MNRAS*, 179, 541
- Rosati P., Borgani S., Norman C., 2002, *ARA&A*, 40, 539
- Rupke D. S., Veilleux S., Sanders D. B., 2005, *ApJS*, 160, 115
- Ruszkowski M., Brüggen M., Begelman M. C., 2004, *ApJ*, 615, 675
- Ruszkowski M., Lee D., Bruggen M., Parrish I., Oh S. P., 2010, *ArXiv e-prints*
- Ruszkowski M., Oh S. P., 2010, *ApJ*, 713, 1332
- Salomé P. et al., 2006, *A&A*, 454, 437
- Sanders D. B., Mirabel I. F., 1996, *ARA&A*, 34, 749
- Sanders J. S., Fabian A. C., 2007, *MNRAS*, 381, 1381
- , 2008, *MNRAS*, 390, L93

- Scannapieco E., Bildsten L., 2005, *ApJ*, 629, L85
- Scannapieco E., Brügger M., 2008, *ApJ*, 686, 927
- Schawinski K., Virani S., Simmons B., Urry C. M., Treister E., Kaviraj S., Kushkuley B., 2009, *ApJ*, 692, L19
- Schaye J. et al., 2010, *MNRAS*, 402, 1536
- Schmidt M., 1968, *ApJ*, 151, 393
- Sijacki D., Springel V., Di Matteo T., Hernquist L., 2007, *MNRAS*, 380, 877
- Silk J., 1977, *ApJ*, 211, 638
- Silk J., Rees M. J., 1998, *A&A*, 331, L1
- Silverman J. D. et al., 2009, *ApJ*, 696, 396
- Silverman J. D. et al., 2008, *ApJ*, 675, 1025
- Smith E. P., Bohlin R. C., Bothun G. D., O’Connell R. W., Roberts M. S., Neff S. G., Smith A. M., Stecher T. P., 1997, *ApJ*, 478, 516
- Soker N., 2006, *New A*, 12, 38
- Somerville R. S., Hopkins P. F., Cox T. J., Robertson B. E., Hernquist L., 2008, *MNRAS*, 391, 481
- Somerville R. S., Primack J. R., Faber S. M., 2001, *MNRAS*, 320, 504
- Springel V., 2005, *MNRAS*, 364, 1105
- Springel V., Di Matteo T., Hernquist L., 2005, *ApJ*, 620, L79
- Springel V., Hernquist L., 2003, *MNRAS*, 339, 289
- Strateva I. et al., 2001, *AJ*, 122, 1861
- Sun M., 2009, *ApJ*, 704, 1586
- Sun M., Jones C., Forman W., Vikhlinin A., Donahue M., Voit M., 2007, *ApJ*, 657, 197
- Teyssier R., Moore B., Martizzi D., Dubois Y., Mayer L., 2011, *MNRAS*, 618
- Tremonti C. A., Moustakas J., Diamond-Stanic A. M., 2007, *ApJ*, 663, L77
- Trump J. R. et al., 2006, *ApJS*, 165, 1
- Urrutia T., Lacy M., Becker R. H., 2008, *ApJ*, 674, 80
- van der Wel A., Bell E. F., Holden B. P., Skibba R. A., Rix H.-W., 2010, *ApJ*, 714, 1779
- Vernaleo J. C., Reynolds C. S., 2006, *ApJ*, 645, 83
- Voit G. M., 2005, *Reviews of Modern Physics*, 77, 207
- Voit G. M., Donahue M., 2005, *ApJ*, 634, 955
- Wang B., Heckman T. M., 1996, *ApJ*, 457, 645
- Weiner B. J. et al., 2005, *ApJ*, 620, 595
- White S. D. M., Rees M. J., 1978, *MNRAS*, 183, 341
- Willmer C. N. A. et al., 2006, *ApJ*, 647, 853
- Xue Y. Q. et al., 2010, *ApJ*, 720, 368
- Zakamska N. L., Narayan R., 2003, *ApJ*, 582, 162